Pathway elucidation and microbial synthesis of proaporphine and bis-benzylisoquinoline alkaloids from sacred lotus (*Nelumbo nucifera*)

Michael E. Pyne [a,b,1,*], Nicholas D. Gold [b,c], & Vincent J. J. Martin [a,b,*]

[a] Department of Biology, Concordia University, Montréal, Québec, Canada

[b] Centre for Applied Synthetic Biology, Concordia University, Montréal, Québec, Canada

[c] Concordia Genome Foundry, Concordia University, Montréal, Québec, Canada

[1] Present address: Department of Biology, Western University, London, Ontario, Canada

*Correspondence and requests for materials should be addressed to:

Michael E. Pyne (email: mpyne3@uwo.ca); and

Vincent J.J. Martin (email: vincent.martin@concordia.ca)

Keywords: Aporphine, benzylisoquinoline, CYP80, lotus, metabolic engineering, norcoclaurine, yeast

ABSTRACT

Sacred lotus (*Nelumbo nucifera*) has been utilized as a food, medicine, and spiritual symbol for nearly 3,000 years. The medicinal properties of lotus are largely attributed to its unique profile of benzylisoquinoline alkaloids (BIAs), which includes potential anti-cancer, anti-malarial and anti-arrhythmic compounds. BIA biosynthesis in sacred lotus differs markedly from that of opium poppy and other members of the Ranunculales, most notably in an abundance of BIAs possessing the (*R*)-stereochemical configuration and the absence of reticuline, a major branchpoint intermediate in most BIA producers. Owing to these unique metabolic features and the pharmacological potential of lotus, we set out to elucidate the BIA biosynthesis network in *N. nucifera*. Here we show that lotus CYP80G (*Nn*CYP80G) and a superior ortholog from Peruvian nutmeg (*Laurelia sempervirens*; *Ls*CYP80G) stereospecifically convert (*R*)-*N*-methylcoclaurine to the proaporphine alkaloid glaziovine, which is subsequently methylated to pronuciferine, the presumed precursor to nuciferine. While sacred lotus employs a dedicated (*R*)-route to aporphine alkaloids from (*R*)-norcoclaurine, we implemented an artificial stereochemical inversion approach to flip the stereochemistry of the core BIA pathway. Exploiting the unique substrate specificity of dehydroreticuline synthase from common poppy (*Papaver rhoeas*) and pairing it with dehydroreticuline reductase enabled *de novo* synthesis of (*R*)-*N*-methylcoclaurine from (*S*)-norcoclaurine and its subsequent conversion to pronuciferine. We leveraged our stereochemical inversion approach to also elucidate the role of *Nn*CYP80A in sacred lotus metabolism, which we show catalyzes the stereospecific formation of the bis-BIA nelumboferine. Screening our collection of 66 plant *O*-methyltransferases enabled conversion of nelumboferine to liensinine, a potential anti-cancer bis-BIA from sacred lotus. Our work highlights the unique

1 benzylisoquinoline metabolism of *N. nucifera* and enables the targeted overproduction of

2 potential lotus pharmaceuticals using engineered microbial systems.

INTRODUCTION

As the national flower of both India and Vietnam, sacred lotus (*Nelumbo nucifera*) has played a major historical role in Asian food, medicine, culture, and religion. Seeds of *N. nucifera* have been consumed for approximately 3,000 years, while most parts of the plant have been used in traditional Chinese medicine to treat fever, diarrhea, cholera, inflammation, and other ailments. The potential health benefits of lotus are largely ascribed to the plant's unique collection of benzylisoquinoline alkaloids (BIAs), which includes many 1-benzylisoquinolines, 15 aporphine alkaloids, seven bis-BIAs, and one unusual tri-BIA (Menéndez-Perdomo and Facchini, 2018; Yang et al., 2018). BIAs produced by sacred lotus exhibit a range of promising pharmacological properties for potential treatment of cancer (neferine and liensinine), malaria (roemerine), arrhythmia (neferine), HIV (norcoclaurine), obesity (pronuciferine), and fungal infection (roemerine). A recent screen of nearly 200 natural products identified the bis-BIA neferine as a pan-coronavirus entry inhibitor with promising *in vitro* activity against the SARS-CoV-2 virus (He et al., 2021).

The sacred lotus BIA metabolic network and its associated metabolites exhibit a number of structural and stereochemical features that are not found in members of the Ranunculales. (*S*)-Reticuline is the major branchpoint intermediate in most BIA-producing plants, giving rise to more than 2,000 derivatized structures within the morphinan, aporphine, protoberberine, phthalideisoquinoline, and benzophenanthridine downstream branches. However, reticuline has not been isolated from sacred lotus, implying that aporphine and bis-BIA pathways branch from *N*-methylcoclaurine or armepavine in *N. nucifera*. Additionally, aporphine alkaloids from *N. nucifera* lack 4′-substitution of the benzyl moiety that derives from 4-hydroxyphenylacetaldehyde in nearly all BIAs elucidated to date (Pyne et al., 2020). An

26 exception is pronuciferine, an unusual proaporphine alkaloid synthesized by lotus, which
27 possesses a 4′-substituted benzyl group, implying the presence of a novel uncharacterized
28 dehydration reaction involved in the conversion of pronuciferine to nuciferine (Menéndez-
29 Perdomo and Facchini, 2018).

30 Beyond structural features, BIAs synthesized by sacred lotus exhibit unique
31 stereochemistry compared to other BIA-producing plants. Most BIAs found in nature are (*S*)-
32 conformers owing to the stereospecific synthesis of (*S*)-norcoclaurine by all norcoclaurine
33 synthase (NCS) orthologs characterized to date. In contrast, sacred lotus synthesizes both (*R*)-
34 and (*S*)-conformers of norcoclaurine. Although the *N. nucifera* genome contains at least five
35 NCS isoforms, a dedicated (*R*)- or (*R*,*S*)-yielding NCS has yet to be identified (Menéndez-
36 Perdomo and Facchini, 2018). (*R*)-*N*-methylcoclaurine and both (*R*)- and (*S*)-stereoisomers of
37 armepavine have also been isolated from sacred lotus (Do et al., 2013; Ka et al., 2010;
38 Kashiwada et al., 2005; Nishibe et al., 1986), suggesting a lack of stereospecificity of BIA
39 methyltransferases from *N. nucifera*. Two such lotus methyltransferases involved in the
40 conversion of norcoclaurine to coclaurine (*Nn*6OMT) and *N*-methylcoclaurine to armepavine
41 (*Nn*OMT5) were recently characterized and shown to methylate both (*S*)- and (*R*)-substrates
42 (Menéndez-Perdomo and Facchini, 2020). All aporphine alkaloids isolated from *N. nucifera* to
43 date possess the (*R*)-configuration, while bis-BIAs from lotus arise from both (*R*)- and (*S*)-
44 precursors or two (*R*)-monomers (Menéndez-Perdomo and Facchini, 2018), highlighting a
45 distinct preference for (*R*)-conformers in downstream branches of the lotus BIA network. These
46 unique structural and stereochemical features of BIA metabolites from *N. nucifera* provide
47 substantial rationale for elucidating BIA biosynthesis in sacred lotus and engineering its
48 production in yeast.

49 Previously, we constructed a yeast BIA platform with capacity to synthesize more than
50 4.5 g/L of plant BIAs (Pyne et al., 2020). Owing to the pharmaceutical potential and unique
51 features of BIA metabolism in sacred lotus, we wished to leverage our BIA production platform
52 for the discovery and engineering of lotus BIA biosynthesis in yeast. In this work we design and
53 implement an artificial pathway to invert the stereochemistry of our high titer BIA production
54 platform. Flipping the stereochemistry of the core BIA pathway enabled access to the bis-BIA
55 and aporphine branches of sacred lotus secondary metabolism. We show that *Nn*CYP80G and
56 *Nn*CYP80A (also referred to as *Nn*CYP80Q1 and *Nn*CYP80Q2) (Nelson and Schuler, 2013) are
57 stereospecific for (*R*)-substrates and catalyze committed steps in the aporphine and bis-BIA
58 branches in sacred lotus. Our work sheds light on the unique BIA metabolism of *N. nucifera* and
59 will enable the pharmacological exploration and overproduction of untapped BIA structures
60 synthesized by sacred lotus.
61

62 # RESULTS

63 ## *De novo* production of armepavine

64 To begin reconstructing the lotus aporphine biosynthesis pathway in yeast, we selected the (*S*)-
65 norcoclaurine-producing strain LP603 as the basis for our work. This strain harbors an
66 overexpressed and deregulated precursor pathway (*ARO4*^{FBR}, *ARO2*, *ARO7*^{FBR}, *TYR1*, *ARO10*),
67 two copies of an optimized (*S*)-norcoclaurine synthase gene (*CjNCSΔN*), and deletion of several
68 key host genes encoding oxidoreductases (*ari1*Δ *adh6*Δ *ypr1*Δ *ydr541c*Δ *gre2*Δ). LP478, the
69 parent of LP603, produces more than 1 g/L of (*S*)-norcoclaurine in a sucrose pulsed fed-batch
70 fermentation (Pyne et al., 2020).

71 Armepavine, a key BIA intermediate in sacred lotus, is synthesized from norcoclaurine
72 via successive action of 6-*O*-methyltransferase (6OMT), coclaurine-*N*-methyltransferase
73 (CNMT), and 7-*O*-methyltransferase (7OMT). Recently, OMT5 from *N. nucifera* (*Nn*OMT5)
74 was characterized from sacred lotus and shown to exhibit 7OMT activity on *N*-methylcoclaurine,
75 yielding armepavine (Menéndez-Perdomo and Facchini, 2020). To engineer LP603 for high-
76 level armepavine production, we introduced a chimeric armepavine production pathway
77 consisting of 6OMT and CNMT from *Papaver somniferum* (*Ps*6OMT and *Ps*CNMT,
78 respectively), in addition to *Nn*OMT5 (**Fig. 1a**). 6OMT and CNMT variants from opium poppy
79 (*P. somniferum*) dramatically outperformed orthologous isoforms from *N. nucifera* (*Nn*6OMT1-
80 4, *Nn*CNMT1, and *Nn*CNMT3) (**Supplementary Fig. 1**). Strain LP609 synthesized 152 mg/L
81 armepavine in small-scale microtiter plate cultivations, corresponding to a 72% consumption of
82 (*S*)-norcoclaurine (**9**) (**Fig. 1b**). A minor amount of (*S*)-coclaurine (**10**) was produced by strain
83 LP609, while a substantial proportion of (*S*)-*N*-methylcoclaurine (**11**) accumulated, indicating
84 incomplete conversion to armepavine by *Nn*OMT5.
85
86 ***Nelumbo nucifera* CYP80G is a stereospecific proaporphine synthase**
87 Having engineered *de novo* synthesis of armepavine (LP609), we set out to characterize the
88 predicted *N. nucifera* aporphine synthase (*Nn*CYP80G) in yeast. However, introduction of
89 *Nn*CYP80G and a cytochrome P450 reductase (CPR) from *Arabidopsis thaliana* (*At*ATR2; strain
90 LP624) failed to alter the metabolite profile of LP609. Swapping *At*ATR2 for a CPR from
91 *Hypericum calycinum* (*Hc*CPR) or including a cytochrome *b5* variant from *Artemisia annua*
92 (*Aa*CYB5) also failed to yield new metabolite peaks consistent with proaporphine or aporphine
93 metabolites.

94 Sacred lotus synthesizes both (*S*)- and (*R*)-conformers of norcoclaurine and armepavine
95 (Menéndez-Perdomo and Facchini, 2018), leading us to speculate that *Nn*CYP80G might be
96 stereospecific. Our armepavine production strain (LP609) employs *Cj*NCSΔN from *Coptis*
97 *japonica*, which we showed yields exclusively (*S*)-norcoclaurine (Pyne et al., 2020), implying
98 that armepavine produced by LP609 is the (*S*)-conformer. To clarify the stereochemistry of BIAs
99 synthesized by strain LP609, we performed chiral analysis on norcoclaurine and armepavine,
100 which were found to be exclusively (*S*)-conformers (**Fig. 1c**). We also detected both (*S*)- and (*R*)-
101 stereoisomers of norcoclaurine and armepavine from commercial extracts of lotus, which is
102 consistent with previous metabolite characterization studies (Menéndez-Perdomo and Facchini,
103 2018).
104 Because LP609 synthesizes exclusively (*S*)-BIAs, yet *N. nucifera* produces both (*S*)- and
105 (*R*)-BIAs, we speculated that *Nn*CYP80G is stereospecific for (*R*)-substrates. To establish the
106 stereospecificity of *Nn*CYP80G, we introduced a partial aporphine production pathway
107 (*Ps*6OMT-*Ps*CNMT-*Nn*OMT5-*Nn*CYP80G-*At*ATR2) to an unmodified BY4741 laboratory
108 strain lacking an NCS enzyme and a dopamine biosynthesis pathway (yielding strain LP626).
109 LP626 is unable to synthesize BIAs *de novo*, thus enabling its use as a host for feeding various
110 stereoisomers of norcoclaurine. Feeding strain LP626 with (*R*,*S*)-norcoclaurine (*rac*-
111 norcoclaurine), generated by the *in vitro* phosphate-catalyzed condensation of dopamine (**1**) and
112 4-hydroxyphenylacetaldehyde (**2**) (Pesnot et al., 2012), yielded (*R*)-armepavine, in addition to
113 (*S*)-armepavine, demonstrating three-step methylation of (*R*)-norcoclaurine (**3**) to (*R*)-
114 armepavine (**6**) by *Ps*6OMT, *Ps*CNMT, and *Nn*OMT5 (**Fig. 1c**). Importantly, feeding *rac*-
115 norcoclaurine to strain LP626 resulted in the formation of a new LC-MS metabolite peak
116 consistent with pronuciferine (**8**) ($[M + H]^+$ = 312.1600 Da) (**Fig. 1d**; dark blue trace). Omitting

117 *Nn*CYP80G failed to generate the tentative pronuciferine LC-MS product. Unexpectedly, feeding
118 (*S*)-norcoclaurine standard to strain LP626 also generated pronuciferine, yet with a peak area
119 approximately 98% smaller than the corresponding peak derived from supplemented *rac*-
120 norcoclaurine (**Fig. 1d**; red trace). Chiral analysis of commercial (*S*)-norcoclaurine revealed that
121 the standard was contaminated with a small quantity of (*R*)-norcoclaurine (**Fig. 1c**), as also
122 shown in a prior study (Pyne et al., 2020), providing explanation for the low level of
123 pronuciferine synthesized by LP626 from supplemented (*S*)-norcoclaurine. Supplementing
124 phosphate buffer in place of *rac*-norcoclaurine and (*S*)-norcoclaurine failed to generate the
125 tentative pronuciferine LC-MS product (**Fig. 1d**).

126 Although an authentic standard of pronuciferine is not available, we detected the same
127 tentative LC-MS peak from commercial lotus leaf extract. Pronuciferine from lotus extract
128 exhibited the same retention time and exact mass as the tentative peak derived from supernatants
129 of strain LP626 supplemented with *rac*-norcoclaurine (**Fig. 1d**; light blue trace). Targeted
130 fragmentation of the tentative pronuciferine peak from lotus extract and supernatants of LP626
131 fed with *rac*-norcoclaurine yielded identical fragmentation spectra (**Fig. 1e**), which were in
132 agreement with published spectra derived from authentic pronuciferine (Bayazeid et al., 2018;
133 Lin et al., 2014).

134 Based on our *rac*-norcoclaurine feeding results (**Fig. 1d**) and prior studies detailing
135 alkaloid isolation (Bishayee et al., 2022; Cao et al., 2022; Yu et al., 2022) and *in vivo* tracer
136 experiments using sacred lotus (Barton et al., 1967; Haynes et al., 1965), we deduced two
137 theoretical routes to pronuciferine (**Fig. 1a**). Because pronuciferine exhibits the same
138 methylation pattern as armepavine, one route involves the direct conversion of (*R*)-armepavine to
139 pronuciferine by *Nn*CYP80G and ATR2. However, based on the mechanism of proaporphine

140 synthesis (Barton and Cohen, 1957), phenol coupling is unable to proceed in 7-*O*-methylated
141 substrates. This mechanism was validated using *in vivo* tracer studies (Barton et al., 1967;
142 Haynes et al., 1965), in which labelled 7-*O*-methylated substrates, such as isococlaurine and
143 armepavine, were not converted to corresponding proaporphine products, while labelled
144 norcoclaurine, coclaurine and *N*-methylcoclaurine substrates were efficiently incorporated.
145 An alternative route to pronuciferine involves conversion of (*R*)-*N*-methylcoclaurine to
146 the proaporphine glaziovine (**7**) and subsequent methylation by *Nn*OMT5, yielding
147 pronuciferine. To clarify the preferred substrate of *Nn*CYP80G and the major route to
148 pronuciferine in sacred lotus, we supplemented (*R*,*S*)-armepavine to strain LP626 harboring a
149 partial proaporphine production pathway (*Ps*6OMT-*Ps*CNMT-*Nn*OMT5-*Nn*CYP80G-*At*ATR2).
150 Whereas feeding 2× SC medium containing (*R*,*S*)-norcoclaurine to LP626 facilitated synthesis of
151 pronuciferine, supplementing (*R*,*S*)-armepavine failed to yield pronuciferine (**Fig. 1d**),
152 corroborating prior evidence that armepavine is not a precursor to proaporphines (Barton et al.,
153 1967). We were also unable to detect synthesis of pronuciferine from supplemented (*R*,*S*)-
154 armepavine by switching to YPD medium or by increasing the pH of 2× SC or YPD medium to
155 7.0, as increasing culture pH improves uptake of BIA metabolites by *S. cerevisiae* (Fossati et al.,
156 2015; Pyne et al., 2016).
157 Owing to the inability of *Nn*CYP80G to convert exogenous (*R*,*S*)-armepavine to
158 pronuciferine, we investigated *Nn*CYP80G activity on *N*-methylcoclaurine, which lacks 7-*O*-
159 methylation, by first deleting the gene encoding *NnOMT5* in LP626, yielding strain LP627. In
160 the absence of *Nn*OMT5, LP627 accumulates (*R*,*S*)-*N*-methylcoclaurine from supplemented
161 (*R*,*S*)-norcoclaurine and is thus unable to synthesize pronuciferine. Feeding (*R*,*S*)-norcoclaurine
162 to LP627 resulted in the formation of a new LC-MS metabolite peak consistent with glaziovine

163 (**7**) ([M + H]$^+$ = 298.1443 Da) (**Fig. 1d**; dark blue trace), a propaporphine alkaloid from *N.*
164 *nucifera* (Cao et al., 2022; Yu et al., 2022). Omitting *Nn*CYP80G or (*R*,*S*)-norcoclaurine failed to
165 generate the tentative glaziovine LC-MS product. We also detected an LC-MS peak from
166 commercial lotus leaf extract with the same retention time and exact mass as the tentative
167 glaziovine peak derived from supernatants of strain LP627 supplemented with *rac*-norcoclaurine
168 (**Fig. 1f**; light blue trace). Targeted fragmentation of the tentative glaziovine peak from
169 supernatants of LP627 fed with *rac*-norcoclaurine yielded fragmentation spectra that were in
170 agreement with published spectra derived from authentic glaziovine (Cao et al., 2022; Yu et al.,
171 2022) (**Fig. 1g**). Importantly, glaziovine accumulation decreased markedly in the presence of
172 *Nn*OMT5, which coincided with the formation of pronuciferine, confirming that proaporphine
173 formation precedes 7-*O*-methylation. Collectively, these data demonstrate that *Nn*CYP80G
174 stereospecifically converts (*R*)-*N*-methylcoclaurine to glaziovine in the committed step of the
175 sacred lotus aporphine biosynthesis pathway.

176 Based on BIA alkaloids isolated from *N. nucifera*, synthesis of nuciferine arises from an
177 unknown dehydration reaction from pronuciferine (Menéndez-Perdomo and Facchini, 2018).
178 Recently, a study of alkaloids from *N. nucifera* identified a cluster of 90 genes closely associated
179 with alkaloid content, including *Nn*CYP80G and several BIA methyltransferases (Yang et al.,
180 2017). However, most of the 90 identified genes do not encode biosynthetic enzymes or encode
181 biosynthetic enzymes, such as methyltransferases, not involved in the conversion of
182 pronuciferine to nuciferine. In an attempt to identify the missing activity, we selected 10 of these
183 candidate biosynthetic genes from lotus (NNU05340, NNU08935, NNU17596, NNU01031,
184 NNU20422, NNU17669, NNU24387, NNU12203, NNU07402, and NNU20868), which were

185 integrated into a pronuciferine-producing strain (LP634). None of the candidate lotus genes
186 facilitated accumulation of nuciferine or consumption of pronuciferine.
187
188 **An artificial *de novo* route to (*R*)-*N*-methylcoclaurine and (*R*)-armepavine using reticuline**
189 **epimerase**
190 Having established a role for *Nn*CYP80G in proaporphine alkaloid biosynthesis using
191 supplementation assays, we aimed to engineer yeast for *de novo* synthesis of pronuciferine.
192 Because lotus ostensibly synthesizes pronuciferine from (*R*)-norcoclaurine in a dedicated (*R*)-
193 specific pathway (**Fig. 1a**) (Menéndez-Perdomo and Facchini, 2018), reconstructing the natural
194 lotus route in yeast would entail screening NCS orthologs from *N. nucifera* and swapping
195 *Cj*NCSΔN for an (*R*)-specific isoform. However, *Cj*NCSΔN dramatically outperformed all NCS
196 variants screened from a diverse array of plants (Bourgeois et al., 2018; Grewal et al., 2021;
197 Pyne and Martin, 2022), enabling high titers (> 4.5 g/L) of BIAs (Pyne et al., 2020).
198 We searched for an alternative route to (*R*)-*N*-methylcoclaurine (**5**) and (*R*)-armepavine
199 (**6**) from (*S*)-norcoclaurine (**9**) and shifted our focus to reticuline epimerase (REPI), an enzyme
200 involved in the committed step of the morphinan BIA pathway (Farrow et al., 2015; Galanie et
201 al., 2015; Winzer et al., 2015). REPI catalyzes the two-step stereochemical inversion of (*S*)- to
202 (*R*)-reticuline via the intermediate 1,2-dehydroreticuline. REPI is composed of dehydroreticuline
203 synthase (DRS) and dehydroreticuline reductase (DRR) domains, which catalyze the respective
204 synthesis and reduction of 1,2-dehydroreticuline. While DRS from opium poppy (*P. somniferum*;
205 *Ps*DRS) is specific for (*S*)-reticuline, DRS from common poppy (*P. rhoeas*; *Pr*DRS) exhibits
206 unique preference for (*S*)-*N*-methylcoclaurine (Farrow et al., 2015), the precursor to armepavine
207 in sacred lotus. We speculated that screening diverse pairs of DRS and DRR orthologs might

208 identify a synthetic DRS-DRR couple capable of catalyzing the stereochemical inversion of (*S*)-
209 to (*R*)-*N*-methylcoclaurine (**Fig. 2a**). A concurrent study employed a similar approach, albeit
210 using supplementation with L-DOPA (Payne et al., 2021). Instead, we wished to develop a fully
211 *de novo* route to (*R*)-*N*-methylcoclaurine and pronuciferine without supplementation of BIA
212 pathway precursors.

213 To engineer a *de novo* stereochemical inversion path to pronuciferine, we first screened
214 several DRS variants for activity on (*S*)-*N*-methylcoclaurine. This screen included *Pr*DRS,
215 *Ps*DRS, DRS from *Chelidonium majus* (*Cm*DRS) and four isoforms from Iranian poppy (*P.*
216 *bracteatum*; *Pb*DRS1-4). *Cm*DRS and *Pb*DRS1-4 share 86-99% identity with the canonical
217 *Ps*DRS variant, whereas *Pr*DRS shares only 79% identity to *Ps*DRS (**Fig. 2b**). In agreement with
218 a prior study (Farrow et al., 2015), *Pr*DRS exhibited remarkable activity on (*S*)-*N*-
219 methylcoclaurine, yielding 1,2-dehydro-*N*-methylcoclaurine (**13**) ($[M + H]^+$ = 298.1443 Da)
220 (**Fig. 2c**).

221 In addition to its reported activity on (*S*)-*N*-methylcoclaurine, we screened *Pr*DRS and
222 other DRS variants on (*S*)-armepavine. Remarkably, *Pr*DRS was the only DRS variant that
223 converted (*S*)-armepavine to 1,2-dehydroarmepavine (**14**) ($[M + H]^+$ = 312.1600 Da) (**Fig. 2c**).
224 Implementation of *Pr*DRS converted nearly 70% of total (*S*)-substrate [combined (*S*)-*N*-
225 methylcoclaurine and (*S*)-armepavine] to dehydro-intermediates. Assuming equivalent LC-MS
226 response factors, the strain harboring *Pr*DRS produced 45-fold more 1,2-dehydro-*N*-
227 methylcoclaurine than 1,2-dehydro-armepavine, although consumption of (*S*)-*N*-
228 methylcoclaurine reduces the pool of available (*S*)-armepavine. Aside from *Pr*DRS, *Ps*DRS
229 consumed 29% of (*S*)-substrates, while the remaining DRS orthologs converted a very small
230 proportion of available (*S*)-conformers to the corresponding dehydro-derivatives.

231 Using *Pr*DRS for synthesis of 1,2-dehydro-BIAs, we next screened DRR variants for
232 reduction of 1,2-dehydro-*N*-methylcoclaurine and 1,2-dehydroarmepavine. Our screen included
233 *Pr*DRR, *Ps*DRR, and two isoforms of DRR from *P. bracteatum* (*Pb*DRR1 and *Pb*DRR2) (**Fig.**
234 **2d**). Introduction of all four DRR orthologs facilitated the near-complete consumption of 1,2-
235 dehydroarmepavine. While none of the DRR variants completely consumed 1,2-dehydro-*N*-
236 methylcoclaurine, strains harboring *Ps*DRR or *Pb*DRR2 each reduced 68% of available
237 substrate. Because authentic (*R*,*S*)-armepavine is commercially available, we utilized (*R*)-
238 armepavine to approximate (*R*)-*N*-methylcoclaurine synthesis, as *Nn*OMT5 catalyzes the
239 methylation of both (*S*)- and (*R*)-conformers of *N*-methylcoclaurine (**Fig. 1c**). Chiral LC-MS
240 analysis of supernatants derived from strains harboring *Pr*DRS and *Ps*DRR revealed synthesis of
241 (*R*)-armepavine, while strains lacking a DRR domain produced exclusively (*S*)-armepavine (**Fig.**
242 **2e**). Importantly, inclusion of *Nn*CYP80G and ATR2 along with *Pr*DRS and *Ps*DRR facilitated
243 *de novo* production of pronuciferine (**Fig. 2d, e**), further establishing the involvement of (*R*)-
244 BIAs in its synthesis. Collectively, these modifications establish an artificial *de novo* route to
245 (*R*)-*N*-methylcoclaurine and pronuciferine via (*S*)-norcoclaurine.
246

247 **Enhancing CYP80G-CPR coupling and probing activity of *Nn*CYP80A**

248 After establishing the role of *Nn*CYP80G in proaporphine alkaloid biosynthesis, we attempted to
249 improve its activity through better coupling to a CPR partner. We assembled a combinatorial
250 CYP80-CPR-CYB5 library by pairing different combinations of plant CPRs and CYB5s with
251 *Nn*CYP80G or *Ls*CYP80G, a predicted CYP80G ortholog from *Laurelia sempervirens* identified
252 from our in-house collection of plant CYPs. We also included in this assay *Nn*CYP80A, a lotus
253 enzyme possessing 80% identity to *Nn*CYP80G. Genes encoding *NnCYP80G* and *NnCYP80A*

254 are adjacent within the lotus genome, suggesting tandem duplication and a potential role for
255 *Nn*CYP80A in BIA biosynthesis (Menéndez-Perdomo and Facchini, 2018). Previous studies
256 have implicated *Nn*CYP80A in bis-BIA biosynthesis, yet its activity has not been experimentally
257 validated. Because all bis-BIAs characterized from lotus derive from at least one (*R*)-monomer,
258 our ability to synthesize both (*S*)- and (*R*)-conformers using *Pr*DRS and DRR provides an
259 opportunity to fully explore *Nn*CYP80A activity.

260 We first assembled a CYP80-CPR-CYB5 library consisting of 24 combinations of one
261 CYP80 (*Nn*CYP80A, *Nn*CYP80G, and *Ls*CYP80G), each paired with one of four CPRs and one
262 of four CYB5s (**Fig. 3a**). We then transformed our 24 strain CYP80-CPR-CYB5 library with a
263 plasmid that expresses both *PrDRS* and *PsDRR* genes for conversion of (*S*)-intermediates to (*R*)-
264 conformers. As we demonstrated above (**Fig. 1d**), all *Nn*CYP80G strains expressing *PrDRS* and
265 *PsDRR* produced pronuciferine (**Fig. 3b**). However, all strains harboring *Ls*CYP80G synthesized
266 more pronuciferine than isogenic strains possessing *Nn*CYP80G. Selection of both CPR and
267 CYB5 variant had a significant effect on pronuciferine production, whereby pronuciferine output
268 was greatest when *Ls*CYP80G was coupled with *Cc*CPR2 and *At*CYB5D.

269 Expression of *PrDRS* and *PsDRR* in strains containing *Nn*CYP80A and different
270 combinations of CPR and CYB5 triggered the formation of a new LC-MS metabolite peak ([M +
271 H]$^+$ = 597.2965 Da) consistent with a high molecular weight bis-BIA product (**Fig. 3c, d**).
272 Selection of both CPR and CYB5 variant had a significant effect on production of the tentative
273 bis-BIA product. The bis-BIA metabolite(s) eluted as a double peak and its formation required
274 *Nn*CYP80A as well as *Pr*DRS and *Ps*DRR (**Fig. 3e**; dark pink trace), indicating a requirement
275 for (*R*)-substrates.

276 At least seven bis-BIAs have been isolated from *N. nucifera* (Menéndez-Perdomo and
277 Facchini, 2018), of which four (nelumborine, nelumboferine, 6-hydroxynorisoliensinine, and *N*-
278 norisoliensinine) have a molecular weight and chemical formula ($C_{36}H_{40}N_2O_6$) consistent with
279 the metabolite peak generated by yeast strains harboring *Nn*CYP80A, *Pr*DRS and *Ps*DRR. Of
280 these tentative products, nelumboferine (**15**) and nelumborine (**16**) possesses a methylation
281 profile consistent with methyltransferases produced by our combinatorial library, as 6-
282 hydroxynorisoliensinine and *N*-norisoliensinine lack methyl groups furnished by *Ps*6OMT and
283 *Ps*CNMT, respectively. Nelumboferine and nelumborine both derive from the coupling of two
284 monomers of *N*-methylcoclaurine (Itoh et al., 2011), indicating that *Nn*OMT5 is not involved in
285 their formation (**Fig. 3d**). To clarify the role of *Nn*OMT5 in the synthesis of the tentative bis-BIA
286 metabolite, we deleted *NnOMT5* from the best performing *Nn*CYP80A strain harboring *At*ATR2
287 and *Pb*CYB5. In agreement with the presumed routes to nelumboferine and nelumborine in *N.*
288 *nucifera*, deletion of *NnOMT5* had no effect on synthesis of the bis-BIA metabolite (**Fig. 3e**;
289 light pink trace).

290 To further probe the identity of the tentative bis-BIA metabolite, we analyzed sacred
291 lotus extracts for the presence of high molecular weight bis-BIA metabolites. We identified a
292 metabolite peak with the same exact mass ($[M + H]^+$ = 597.2965 Da) and retention time in lotus
293 leaf extract as the tentative bis-BIA product synthesized by yeast strains harboring *Nn*CYP80A,
294 *Pr*DRS and *Ps*DRR (**Fig. 3e**; green trace). In line with yeast strains expressing *NnCYP80A,*
295 *PrDRS* and *PsDRR*, the lotus bis-BIA metabolite eluted as a double peak in commercial lotus
296 extract. Targeted fragmentation of the tentative bis-BIA product from lotus extract and yeast
297 supernatants yielded several common fragment ions, notably $[M + H]^+$ = 192.1, 475.2, 554.2,
298 and 566.2 Da (**Fig. 3f**).

299 We also screened the CYP80-CPR-CYB5 combinatorial strain library in the absence of a
300 DRS-DRR pair to search for tentative products arising from exclusively (*S*)-metabolites. In
301 agreement with known stereochemistry of lotus alkaloids (Menéndez-Perdomo and Facchini,
302 2018), no tentative bis-BIA or proaporphine metabolite peaks were identified, confirming an
303 inability of *Nn*CYP80A, *Nn*CYP80G, and *Ls*CYP80G to turnover substrates possessing
304 exclusively (*S*)-configurations.

305 Guattegaumerine (**17**) is a bis-BIA metabolite synthesized by *Berberis stolonifera*. Both
306 guattegaumerine and nelumboferine derive from two units of (*R*)-*N*-methylcoclaurine, yet
307 guattegaumerine derives from 3′-*O*-4′ phenol coupling, while nelumboferine arises from 7-*O*-3′
308 coupling (**Fig. 3d**). Recently, yeast was engineered to synthesize guattegaumerine from (*R*)-*N*-
309 methylcoclaurine by employing CYP80A1 from *B. stolonifera* (*Bs*CYP80A1), the product of
310 which was validated using authentic guattegaumerine standard (Payne et al., 2021). Because
311 guattegaumerine, nelumboferine, and nelumborine are structural isomers ($C_{36}H_{40}N_2O_6$) generated
312 through different phenol coupling reactions, we reasoned that our *Nn*CYP80A-derived bis-BIA
313 product would yield a similar LC-MS retention time and MS/MS fragmentation spectra to that of
314 *Bs*CYP80A1-derived guattegaumerine. To first demonstrate synthesis of guattegaumerine, we
315 paired *Bs*CYP80A1 with four CPR variants in our (*R*)-*N*-methylcoclaurine host lacking
316 *NnOMT5*. All *Bs*CYP80A1 strains facilitated the synthesis of a new LC-MS peak with the same
317 exact mass as guattegaumerine ($[M + H]^+$ = 597.2965 Da) (**Fig. 3e**; black trace). Pairing of
318 *Bs*CYP80A1 with *Hc*CPR yielded approximately 45-fold more guattegaumerine than an isogenic
319 strain harboring *Cc*CPR2 (**Supplementary Fig. 2**). Production of guattegaumerine required
320 expression of *PrDRS* and *PsDRR*, corroborating the requirement for (*R*)-*N*-methylcoclaurine by
321 *Bs*CYP80A1 (Payne et al., 2021). In contrast to the *Nn*CYP80A-derived bis-BIA product,

322 guattegaumerine eluted as a single LC-MS peak, yet with the same retention time as the
323 *Nn*CYP80A product, presumably due to the different phenol coupling reactions involved in the
324 synthesis of guattegaumerine, nelumboferine, and nelumborine. We compared MS/MS
325 fragmentation of *Nn*CYP80A- and *Bs*CYP80A1-derived products (**Fig. 3f**), which yielded the
326 same major 597→192 transition generated by fragmentation of authentic guattegaumerine
327 standard (Payne et al., 2021). Collectively, these data are consistent with a tentative assignment
328 of nelumboferine or nelumborine for the identity of the *Nn*CYP80A-derived bis-BIA product.
329

330 **Derivatization of nelumboferine by screening a library of BIA *O*-methyltransferases**

331 In sacred lotus, nelumboferine (**15**) is converted to liensinine (**18**) or isoliensinine (**19**) via
332 methylation by 7OMT or 4′OMT, respectively (Itoh et al., 2011). One or both of these
333 compounds are subsequently methylated to give neferine (**20**) (**Fig. 4a**). We screened our in-
334 house library of BIA methyltransferase enzymes for activity on nelumboferine. In total we
335 introduced 66 putative *O*-methyltransferases from 19 BIA-producing plant species to our top-
336 performing *Nn*CYP80A strain (**Fig. 4b**). Our search included seven predicted *O*-
337 methyltransferases from *N. nucifera* (*Nn*6OMT1-4 and *Nn*7OMT1-3).

338 We analyzed cultures of methyltransferase-expressing strains for new peaks consistent
339 with single ($[M + H]^+$ = 611.3121 Da) or double methylation ($[M + H]^+$ = 625.3278 Da) of the
340 *Nn*CYP80A-derived bis-BIA product ($[M + H]^+$ = 597.2965 Da). One *O*-methyltransferase
341 candidate (*Ec*OMT1 from *Eschscholzia californica*) generated a peak ($[M + H]^+$ = 611.3121 Da)
342 consistent with single methylation (**Fig. 4c**). Based on a prior study, *Ec*OMT1 is a 7OMT that
343 catalyzes the conversion of reticuline to laudanine (Fujii et al., 2007). In line with its reported
344 activity, *Ec*OMT1 clusters with other enzymes exhibiting confirmed or predicted 7OMT activity

345 (**Fig. 4b**), including *Ec*OMT2, a scoulerine 9OMT (SOMT) that also possesses 7OMT activity
346 on reticuline (Purwanto et al., 2017). We analyzed the active site of *Ec*OMT1 using AlphaFold
347 (Jumper et al., 2021; Varadi et al., 2022) and observed a unique Gly256 residue that is predicted
348 to form a hydrogen bond with the His259 catalytic residue (**Supplementary Fig. 3**) conserved
349 across all BIA OMTs (Morris and Facchini, 2019). Gly256 is substituted with a bulky Trp
350 residue in other closely related BIA OMTs within the *Ec*OMT1- and *Ec*OMT2-containing 7OMT
351 clade, which might hinder binding of large bis-BIA substrates. Similarly, Gly308 of *Ec*OMT1 is
352 believed to play a role in the alleviation of substrate steric hindrance (Morris and Facchini, 2019)
353 and related 7OMTs harbor a bulkier Ile, Leu, or Val residue in this position.
354 Based on the reported 7OMT activity of *Ec*OMT1, the identity of the new methylated
355 LC-MS product is expected to be liensinine ($C_{37}H_{42}N_2O_6$) (**Fig. 4a**), a major bis-BIA in lotus.
356 We obtained authentic liensinine standard, which generated a mass ($[M + H]^+$ = 611.3121 Da)
357 and retention time (RT = 2.16 min) in agreement with the LC-MS product derived from
358 *Ec*OMT1 activity on nelumboferine (**Fig. 4c**). We also compared MS/MS fragmentation of the
359 tentative liensinine metabolite peak with authentic liensinine standard, which generated identical
360 fragmentation spectra (**Fig. 4d**). Specifically, the major fragment ion with mass $[M + H]^+$ =
361 206.1 was previously used to differentiate liensinine from its isomer isoliensinine ($C_{37}H_{42}N_2O_6$)
362 (Zhou et al., 2007), which arises from 4′-*O*-methylation of nelumboferine in place of 7-*O*-
363 methylation. The fragment ion with mass $[M + H]^+$ = 206.1 also differentiates liensinine from its
364 nelumboferine precursor ($C_{36}H_{40}N_2O_6$), which yields a corresponding fragment ion with mass [M
365 $+ H]^+$ = 192.1 (**Fig. 3f, g**), indicating *O*-methylation of the free tetrahydroisoquinoline moiety of
366 nelumboferine. Importantly, synthesis of liensinine by yeast strains harboring *Nn*CYP80A,
367 ATR2, and *Ec*OMT1 confirms that nelumboferine is a product of CYP80A from *N. nucifera*.

368 We also identified liensinine in commercial lotus extract (RT = 2.16 min), although an
369 additional larger peak (RT = 2.25 min) with the same mass was also observed (**Fig. 4c**). As
370 expected, MS/MS fragmentation of the minor lotus peak yielded the key 611 → 206 transition
371 characteristic of liensinine (**Fig. 4e;** dark green). In contrast, fragmentation of the dominant lotus
372 product (RT = 2.25 min) yielded a major 611 → 192 transition (**Fig. 4e;** light green), which is in
373 agreement with isoliensinine (Zhou et al., 2007).
374 We also introduced our panel of 66 methyltransferases to our guattegaumerine-producing
375 strain harboring *Bs*CYP80A1 and *Hc*CPR, yet were unable to detect methylated derivatives ([M
376 + H]$^+$ = 611.3121 Da or 625.3278 Da). Our screen identified several methyltransferases with
377 tentative 7OMT or 4′OMT activities on *N*-methylcoclaurine (**Supplementary Table 1**).
378

379 # DISCUSSION

380 In contrast to most BIA-producing plants, in which the core BIA pathway proceeds through
381 exclusively (*S*)-conformers, sacred lotus synthesizes (*R*)-*N*-methylcoclaurine and (*R*)-armepavine
382 in a dedicated (*R*)-stereochemical path from (*R*)-norcoclaurine. In this study, we designed and
383 implemented a synthetic strategy to flip the stereochemistry of our BIA platform strain by
384 exploiting the unique substrate preference of DRS from common poppy (*Pr*DRS). Pairing of
385 *Pr*DRS with several DRR variants enabled stereochemical inversion of (*S*)-*N*-methylcoclaurine
386 and (*S*)-armepavine via 1,2-dehydro-*N*-methylcoclaurine and 1,2-dehydro-armepavine
387 intermediates. Production of (*R*)-conformers enabled the characterization of *Nn*CYP80G and
388 *Nn*CYP80A as respective stereospecific proaporphine and bis-BIA synthases involved in the
389 committed steps of the aporphine and bis-BIA branches of BIA metabolism in sacred lotus.

390 Our findings firmly establish roles for *Nn*CYP80G and *Nn*CYP80A in propaporphine and
391 bis-BIA biosynthesis, respectively. Specifically, we show that *Nn*CYP80G is a proaporphine
392 synthase that catalyzes the stereospecific conversion of (*R*)-*N*-methylcoclaurine to glaziovine,
393 which is subsequently methylated to pronuciferine by *Nn*OMT5. Formation of pronuciferine was
394 dependent on implementation of *Pr*DRS-*Ps*DRR or exogenous supplementation of (*R*,*S*)-
395 norcoclaurine, clearly establishing the stereospecificity of *Nn*CYP80G for (*R*)-*N*-
396 methylcoclaurine. Our findings, coupled with the recent discovery and characterization of
397 *Nn*OMT5 (Menéndez-Perdomo and Facchini, 2020), the dedicated 7OMT responsible for
398 armepavine and pronuciferine production, have unlocked the aporphine branch of BIA
399 biosynthesis in sacred lotus. Our data is in agreement with the phenol coupling mechanism of
400 aporphine formation set forth by Barton and Cohen in 1957, in which the authors predicted the
401 existence of proaporphine (dienone) intermediates prior to the isolation of any such metabolites
402 from natural sources (Barton and Cohen, 1957). Soon after, many proaporphine natural products
403 were isolated from plants, including pronuciferine, mecambrine, stepharine, crotonosine, and
404 glaziovine (Stuart and Cava, 1968). According to the phenol coupling mechanism, 7-*O*-
405 methylated substrates, such as isococlaurine and armepavine, are not converted into
406 proaporphine structures, which was validated using *in vivo* tracer studies (Barton et al., 1967;
407 Haynes et al., 1965). Our findings from yeast supplementation assays are in agreement with this
408 general mechanism, as feeding (*R*,*S*)-norcoclaurine, but not (*R*,*S*)-armepavine, facilitated
409 synthesis of pronuciferine, suggesting that *Nn*CYP80G acts on a substrate upstream of
410 armepavine. By deleting *Nn*OMT5, we showed that *Nn*CYP80G catalyzes the formation of
411 glaziovine from (*R*)-*N*-methylcoclaurine based on exogenous supplementation of (*R*,*S*)-
412 norcoclaurine. While glaziovine is not a major constituent of sacred lotus (Menéndez-Perdomo

413 and Facchini, 2018), several recent studies have reported its isolation from seeds of *N. nucifera*
414 (Bishayee et al., 2022; Cao et al., 2022; Yu et al., 2022). In contrast, glaziovine is a major
415 alkaloid in *Ocotea glaziovii* and other select species of Lauraceae and Annonaceae (Agnès et al.,
416 2022). Our demonstration of glaziovine synthesis coupled with the inability of *Nn*CYP80G to act
417 on exogenous (*R*,*S*)-armepavine confirms that proaporphine synthesis precedes 7-*O*-methylation
418 in agreement with the proposed phenol coupling mechanism (Barton and Cohen, 1957).
419 Although a recent study failed to demonstrate *Nn*OMT5 activity on aporphine substrates and thus
420 postulated that 7OMT precedes aporphine synthesis (Menéndez-Perdomo and Facchini, 2020),
421 glaziovine and other proaporphine metabolites were not assayed. We show that *Nn*OMT5
422 exhibits appreciable activity on both 1-benzylisoquinoline (*N*-methylcoclaurine) and
423 proaporphine substrates (glaziovine), indicating that *N*-methylcoclaurine is the major
424 branchpoint metabolite in sacred lotus and 7-*O*-methylation acts as a blocking group to limit flux
425 to the aporphine pathway.

426 Nuciferine, a major alkaloid in *N. nucifera* and a metabolite with potential anti-cancer
427 properties, possesses the same methylation pattern as pronuciferine, indicating that a hitherto
428 unidentified enzyme is responsible for conversion of pronuciferine to nuciferine. To identify the
429 unknown activity, we implemented 10 lotus metabolic enzymes with expression profiles similar
430 to *Nn*CYP80G and other core BIA pathway enzymes. However, we were unable to identify the
431 elusive missing enzyme responsible for the conversion of pronuciferine to nuciferine. More
432 sophisticated enzyme discovery strategies, such as those employed in the recent elucidation of
433 colchicine and strychnine biosynthetic pathways (Hong et al., 2022; Nett et al., 2020), will be
434 required to complete the lotus pathway to nuciferine.

435 *Nn*CYP80A was previously implicated in bis-BIA biosynthesis, while other studies have
436 proposed it to be an alternative isoform of *Nn*CYP80G (Menéndez-Perdomo and Facchini,
437 2018). We leveraged our artificial stereochemical inversion strategy to clarify the role of
438 *Nn*CYP80A in sacred lotus metabolism. We show that *Nn*CYP80A is the dedicated bis-BIA
439 synthase involved in the committed step of the *N. nucifera* bis-BIA biosynthesis pathway. To
440 date seven high molecular weight bis-BIA metabolites have been isolated from sacred lotus, in
441 addition to an unusual tri-BIA (neoliensinine) (Menéndez-Perdomo and Facchini, 2018). Of the
442 characterized lotus bis-BIAs, only nelumboferine and nelumborine possess the exact mass ([M +
443 H]$^+$ = 597.2965 Da; $C_{36}H_{40}N_2O_6$) and methylation profile consistent with the *Nn*CYP80A-
444 catalyzed metabolite. Nelumborine and nelumboferine possess the same methylation pattern yet
445 derive from distinct phenol coupling reactions. Whereas nelumboferine and other lotus bis-BIAs
446 derive from a C7-*O*-C3′ phenol coupling, nelumborine arises from an unusual C8-C3′ coupling.
447 We showed that formation of the *Nn*CYP80A bis-BIA product was independent of *Nn*OMT5, yet
448 required the presence of *Pr*DRS-*Ps*DRR, implicating involvement of (*R*)-*N*-methylcoclaurine in
449 its synthesis. Consistent with this observation, nelumboferine arises from two units of (*R*)-*N*-
450 methylcoclaurine (Itoh et al., 2011; Nishimura et al., 2013), while to our knowledge the
451 stereochemistry of *N*-methylcoclaurine monomers in the synthesis of nelumborine has not been
452 deduced.

453 Based on the methylation profile of BIAs isolated from *N. nucifera*, nelumboferine gives
454 rise to neferine, the fully methylated bis-BIA end product in lotus, via convergent routes from
455 liensinine or isoliensinine (Itoh et al., 2011) involving unidentified 7OMT and 4′OMT enzymes.
456 We introduced our library of 66 plant methyltransferases into our top bis-BIA-producing strain,
457 including seven predicted OMTs from *N. nucifera*, and identified *Ec*OMT1 from California

458 poppy (*Eschscholzia californica*) as a promiscuous 7OMT with activity on nelumboferine. To
459 our knowledge, this is the first plant OMT capable of methylating bis-BIAs and we identified
460 two unique *Ec*OMT1 active site residues (Gly256 and Gly308) that are not conserved across
461 closely related plant 7OMT orthologs, such as *Ec*OMT2. These residues might play a role in
462 positioning the nelumboferine substrate or alleviating steric hindrance of bulky bis-BIAs (Morris
463 and Facchini, 2019). Interestingly, *Ec*OMT1 did not exhibit 7OMT activity on guattegaumerine,
464 which likely reflects the distinct conformations adopted by guattegaumerine and nelumboferine
465 isomers. Implementation of *Ec*OMT1 in a strain containing *Nn*CYP80A, ATR2, *Pr*DRS, and
466 *Ps*DRR facilitated synthesis of liensinine, which was confirmed using an authentic liensinine
467 standard. Liensinine is a major bis-BIA metabolite in sacred lotus with promising anti-cancer
468 activity (Zhou et al., 2015) and our findings establish an artificial *de novo* path for microbial
469 overproduction of liensinine. While we did not identify the dedicated *N. nucifera* bis-BIA 7OMT
470 involved in liensinine formation, our findings might aid in the identification of the elusive
471 enzyme by using *Ec*OMT1 to query the lotus genome, which encodes at least 60 candidate *O*-
472 methyltransferase genes (Li et al., 2021). Moreover, repeating our screen of diverse plant *O*-
473 methyltransferases might unveil a novel 4′OMT variant with activity on liensinine, thus enabling
474 synthesis of neferine, another prospective anti-cancer pharmaceutical.

475 Formation of liensinine by the concerted activity of *Nn*CYP80A and *Ec*OMT1 further
476 confirms nelumboferine as a product of CYP80A activity in *N. nucifera*. We compared
477 *Nn*CYP80A activity to that of *Bs*CYP80A1, a recently characterized bis-BIA synthase from
478 *Berberis stolonifera*. *Bs*CYP80A1 catalyzes the 3′-4′ C-O phenol coupling of two units of (*R*)-*N*-
479 methylcoclaurine to give guattegaumerine or one unit each of (*R*)- and (*S*)-*N*-methylcoclaurine,
480 yielding berbamunine (Payne et al., 2021). Products of *Bs*CYP80A1 and *Nn*CYP80A possess the

481 same mass ([M + H]$^+$ = 597.2965 Da; $C_{36}H_{40}N_2O_6$) and expected methylation profile, yet the
482 *Nn*CYP80A product eluted as two distinct LC-MS peaks, while strains harboring *Bs*CYP80A1
483 produced a single peak. Although we confirmed nelumboferine as a product of *Nn*CYP80A
484 based on conversion to liensinine, it is possible that *Nn*CYP80A is involved in the biosynthesis
485 of both nelumboferine and nelumborine by catalyzing dual coupling reactions (C7-*O*-C3′ and
486 C8-C3′, respectively), which might provide justification for the two LC-MS peaks derived from
487 *Nn*CYP80A activity. However, the biosynthetic origin of nelumborine in *N. nucifera* remains
488 unclear.

489 *NnCYP80A* and *NnCYP80G* genes are adjacent in the genome of *N. nucifera*, suggesting
490 a tandem duplication event. Despite different roles in BIA metabolism, the respective
491 *Nn*CYP80A and *Nn*CYP80G enzymes share a significantly higher degree of sequence identity
492 (80% amino acid identity) than *Bs*CYP80A1 and *Nn*CYP80A bis-BIA synthases (45% amino
493 acid identity), both of which catalyze the coupling of two units of (*R*)-*N*-methylcoclaurine.
494 Surprisingly, based on amino acid sequence, *Bs*CYP80A1 is more closely related to lotus
495 *Nn*CYP80G aporphine synthase than the analogous lotus *Nn*CYP80A bis-BIA synthase. Owing
496 to their similarity, earlier studies assumed that *Nn*CYP80G and *Nn*CYP80A (also referred to as
497 *Nn*CYP80Q1 and *Nn*CYP80Q2) (Nelson and Schuler, 2013) both encode bis-BIA synthases.
498 Instead, our findings suggest that following gene duplication, *Nn*CYP80A and *Nn*CYP80G
499 diverged in activity. These observations suggest that it might be possible to switch *Nn*CYP80G
500 to a bis-BIA synthase or *Nn*CYP80A to an aporphine synthase with a potentially small number
501 of amino acid changes. Our characterization of *Nn*CYP80A and *Nn*CYP80G adds to the diverse
502 collection of plant CYP80 variants, including corytuberine synthase (CYP80G2), (*S*)-*N*-
503 methylcoclaurine 3′-hydroxylase (CYP80B1), and CYP80F1 involved in littorine rearrangement,

504 with key roles in benzylisoquinoline and tropane alkaloid metabolism. An in-depth structural
505 analysis of such broad CYP80 enzymes is likely to shed light on key residues involved in
506 substrate binding and catalytic mechanism.

507 In addition to *Nn*CYP80A and *Bs*CYP80A1 variants, Asian moonseed (*Menispermum*
508 *dauricum*) and Canadian moonseed (*M. canadense*) synthesize dauricine, a potential anti-cancer
509 bis-BIA that arises from the C3′-*O*-C4′ coupling of two units of (*R*)-armepavine. A previous
510 study screened five plant CYP80A orthologs in an (*R*)-armepavine-producing strain, yet did not
511 observe production of dauricine (Payne et al., 2021). We attempted to devise an artificial route to
512 dauricine through direct methylation of guattegaumerine by screening our library of 66 plant
513 methyltransferases in a strain harboring *Bs*CYP80A1 and *Hc*CPR. However, we were also
514 unsuccessful in synthesizing dauricine or methylated derivatives of guattegaumerine. A more
515 exhaustive screen of diverse plant CYP80A orthologs on stereoisomers of both *N*-
516 methylcoclaurine and armepavine might unveil new coupling activities, such as the C3′-*O*-C4′
517 coupling route of (*R*)-armepavine in the biosynthesis of dauricine.

518 To the best of our knowledge, a dedicated (*R*)- or (*R*,*S*)-yielding NCS has yet to be
519 identified from sacred lotus, which prompted our artificial route involving *Pr*DRS and *Ps*DRR
520 (REPI). While our stereochemical inversion approach enabled the use of the highly active (*S*)-
521 specific *Cj*NCSΔN variant (Grewal et al., 2021; Pyne et al., 2020), the native lotus route from
522 (*R*)-norcoclaurine bypasses the requirement of DRS and DRR enzymes. Thus, it is unclear if our
523 stereochemical inversion path is more efficient than the native route when reconstructed in
524 engineered yeast. Screening all five of the predicted lotus NCS variants (Menéndez-Perdomo and
525 Facchini, 2018) might lead to the discovery of the presumed (*R*)-specific isoform. Relatedly, we
526 showed that two lotus CNMT variants (*Nn*CNMT1 and *Nn*CNMT3) lacked activity in a

527 *Cj*NCSΔN strain, suggesting that these enzymes might be specific for (*R*)-substrates or
528 remaining unidentified lotus methyltransferases are involved in (*R*)-*N*-methylcoclaurine
529 synthesis. Consequently, several core enzymes involved in the (*R*)-specific BIA pathway remain
530 unidentified in *N. nucifera*.

531 Finally, our study highlights the utility of high-titer microbial strains in plant enzyme
532 discovery and pathway elucidation. BIA output from our (*S*)-norcoclaurine strain exceeds 1.5 g/L
533 (Pyne et al., 2020), which provides an ideal background for enzyme characterization, particularly
534 those with poor catalytic properties or weak off-target activities. By repurposing our BIA
535 platform, we achieved *de novo* synthesis of 152 mg/L armepavine, a 14-fold improvement over a
536 previous study (11.1 mg/L armepavine) in which L-DOPA precursor supplementation was
537 employed to boost BIA synthesis (Payne et al., 2021). Relatedly, guattegaumerine output varied
538 by a factor of 45 across all four of our *Bs*CYP80A1-CPR strains, while an earlier study was
539 unable to detect guattegaumerine in two out of four CPR pairings (Payne et al., 2021). We also
540 detected pronuciferine or bis-BIA synthesis from all 24 strains of our combinatorial CYP80-
541 CPR-CYB5 library, again showcasing the utility of our high titer BIA platform in the discovery
542 and elucidation of plant secondary metabolic pathways. Our characterization of both *Nn*CYP80A
543 and *Nn*CYP80G herein will enable the exploration and overproduction of potential aporphine
544 and bis-BIA therapeutics from sacred lotus, such as nuciferine, liensinine, and neferine.

545

546 **Acknowledgments**

547 We thank the Concordia Genome Foundry for assistance with combinatorial strain construction
548 and Marcos DiFalco and Lauren Narcross for assistance with LC-MS analyses. This study was

549 financially supported by an NSERC-Industrial Biocatalysis Network (IBN) grant and an NSERC
550 Discovery grant. M.E.P. was supported by an NSERC Postdoctoral Fellowship. V.J.J.M. is
551 supported by a Concordia University Research Chair.
552

553 **Author contributions**

554 M.E.P. designed the research and performed the experiments with supervision from V.J.J.M.
555 N.D.G. assisted with combinatorial pathway assembly and LC-MS analyses. M.E.P. and V.J.J.M.
556 wrote the manuscript.
557

558 **Competing financial interests**

559 The authors declare no competing financial interests.
560

561 **Additional information**

562 Supplementary information is available in the online version of the paper. Correspondence and
563 requests for materials should be addressed to M.E.P. and V.J.J.M.
564

565 **Data availability**

566 Data supporting the findings of this work are available within the paper and its SI Appendix.
567 Source data for the figures in this paper and the SI Appendix are provided in Dataset S1.
568

569 # METHODS

570 **Chemicals and reagents.** General chemicals and reagents were purchased commercially,
571 including dopamine (Sigma-Aldrich), (*S*)-norcoclaurine (Toronto Research Chemicals), 4-
572 hydroxyphenylacetaldehyde (Toronto Research Chemicals), liensinine (MedChemExpress), and
573 (*R*,*S*)-armepavine (MuseChem), unless stated otherwise. Lotus leaf extract was purchased from
574 Amazon (Plum Flower Brand He Ye) or eBay (Hawaii Pharm Pink Lotus herbal extract).

575 **Plasmids, strains, and growth media.** The quadruple auxotrophic *S. cerevisiae* strain BY4741
576 (*MATa his3Δ1 leu2Δ0 met15Δ0 ura3Δ0*) is the origin of all engineered strains in this study.
577 Strain LP478 was utilized as the basis for this work (Pyne et al., 2020). Cultures were grown in
578 YPD (10 g/L Bacto Yeast Extract, 20 g/L Bacto peptone, 20 g/L glucose) or synthetic complete
579 (SC) medium [6.7 g/L Difco Yeast Nitrogen Base (YNB) without amino acids, 1.62-1.92 g/L
580 Drop-out Medium Supplements (Millipore-Sigma) minus appropriate amino acids, 20 g/L
581 glucose). Recombinant cells were selected on YPD agar containing 400 μg/mL G418, 200
582 μg/mL hygromycin B, or 200 μg/mL of each antibiotic. Selection using auxotrophic markers was
583 performed in SC medium lacking histidine. Oligonucleotides utilized in this study are listed in
584 Dataset S2. Plasmids and strains employed in this work are provided in **Supplementary Tables**
585 **2** and **3**, respectively.

586 **Yeast strain construction.** Genetic modifications to yeast were made via CRISPR-Cas9-
587 mediated genomic integration (Horwitz et al., 2015; Ryan et al., 2014) and *in vivo* DNA
588 assembly (Shao et al., 2009). Cas9 and gRNA were delivered to yeast using pCas-G418 (ref.
589 (Ryan et al., 2014)) or pCas-Hyg (ref. (Bean et al., 2022)). Linear gRNA cassettes were
590 retargeted by PCR and assembled using *in vivo* gap repair with a BsaI- and NotI-digested pCas
591 backbone (Bean et al., 2022). Roughly 150 ng of digested pCas was combined with 300 ng of

592 linear gRNA cassette and 500-1,000 ng of total repair DNA in a standard 50 µL lithium acetate
593 transformation. Cells were heat-shocked at 42 °C for 30 minutes, recovered for 16 hours, and
594 plated onto yeast agar plates containing appropriate antibiotics. Both linear pCas-G418 and
595 pCas-Hyg plasmids were used for complex multi-part DNA assemblies. The CYP80-CPR-CYB5
596 combinatorial library was assembled using the Echo 550 acoustic liquid handler. Design of
597 gRNAs was performed by selecting top hits common to both CCTop (Labuhn et al., 2017) and a
598 yeast CRISPRi web tool (Smith et al., 2016). Chromosomal loci for DNA integration were
599 selected from previous studies (Bai Flagfeldt et al., 2009; Bourgeois et al., 2018; Mikkelsen et
600 al., 2012; Reider Apel et al., 2016). Gene expression cassettes and genomic integration sites
601 utilized in this work are listed in **Supplementary Tables 4** and **5**, respectively. Synthetic DNAs
602 employed in this study are provided in **Dataset S3**. The yeast *GRE2* gene was replaced with a
603 synthetic DNA landing pad (LP5.T3) possessing a unique Cas9 target site (T3).
604 **Microtiter plate assay for BIA quantification.** Colonies were picked in triplicate into 0.5 mL
605 of 2× SCS medium (13.4 g/L Difco Yeast Nitrogen Base (YNB) without amino acids, 2× Drop-
606 out Medium Supplements (Millipore-Sigma), 40 g/L sucrose) within 96-well deep well plates.
607 Following 24 h of growth, cultures were back-diluted 50× into 0.5 mL of fresh 2× SCS medium
608 in 96-well deep well plates. Cultures were grown at 30 °C with shaking at 350 rpm. Following
609 48-72 h of growth, OD_{600} measurements were taken, and culture broth was stored at -20 °C for
610 subsequent analysis by LC-MS.
611 **LC-MS and chiral analysis of BIA metabolites.** BIA metabolites were extracted from culture
612 broth containing cells and growth medium. Seven µL of culture broth was combined with 27 µL
613 of 100% acetonitrile (ACN). Following five minutes of shaking at room temperature, 146 µL of
614 0.12% formic acid was added to give a final concentration of 15% ACN and 0.1% formic acid.

615 Samples were diluted an additional 10-fold in 15% ACN and 0.1% formic acid. Samples were
616 centrifuged at 4,000 RCF and 10 μL of extracted culture supernatant was separated on a 1290
617 Infinity II LC system (Agilent Technologies). Metabolites were separated using the following
618 gradient: 2% B to 10% B from 0-4 min (0.3 mL/min), 10% B to 85% B from 4-6 min (0.3
619 mL/min), held at 85% B from 6-7 min (0.3 mL/min), 85% B to 2% B from 7-7.1 min (0.3
620 mL/min), and held at 2% B from 7.1-9 min (0.45 mL/min). Solvent A was 0.1% formic acid in
621 water and solvent B was 0.1% formic acid in 100% ACN. Following separation, eluent was
622 injected into an Agilent 6545 quadrupole time-of-flight MS (QTOF-MS; Agilent Technologies)
623 equipped with a Zorbax Eclipse Plus C18 column (50 × 2.1 mm, 1.8 μm; Agilent Technologies).
624 The sample tray and column compartment were set to 4 °C and 30 °C, respectively. The sheath
625 gas flow rate and temperature were adjusted to 10 L/min and 350 °C, respectively, while drying
626 and nebulizing gases were set to 12 L/min and 55 psig, respectively. The drying gas temperature
627 was set to 325 °C. QTOF data was processed and manipulated using Agilent MassHunter
628 Qualitative Analysis software. Norcoclaurine ($[M + H]^+$ = 272.1287 Da), coclaurine ($[M + H]^+$ =
629 286.1443 Da), *N*-methylcoclaurine ($[M + H]^+$ = 300.1600 Da), armepavine ($[M + H]^+$ =
630 314.1756 Da), 1,2-dehydro-*N*-methylcoclaurine ($[M + H]^+$ = 298.1443 Da), and 1,2-
631 dehyroarmepavine ($[M + H]^+$ = 312.1600 Da) were identified by exact mass. Norcoclaurine and
632 armepavine were quantified using authentic standards. Pronuciferine ($[M + H]^+$ = 312.1600 Da),
633 glaziovine ($[M + H]^+$ = 298.1443 Da), and nelumboferine ($[M + H]^+$ = 597.2965 Da) were
634 identified by retention time, exact mass, and MS/MS fragmentation by comparison to extracts
635 from leaves of *N. nucifera*. Guattegaumerine ($[M + H]^+$ = 597.2965 Da) was identified by exact
636 mass and MS/MS fragmentation. Liensinine ($[M + H]^+$ = 611.3121 Da) was identified by
637 retention time, exact mass, and MS/MS fragmentation by comparison to an authentic standard.

638 MS/MS fragmentation of glaziovine, pronuciferine, and guattegaumerine were compared against
639 published fragmentation spectra.

640 Chiral analysis of norcoclaurine and armepavine was performed by modifying an existing
641 method. Culture supernatant from yeast strains grown in deep-well plates were centrifuged to
642 remove debris and diluted 1:50 or 1:100 in H_2O. Ten µL was loaded onto a SHODEX ORPak
643 CDBS-453 column and separated chromatographically using a 1290 Infinity II HPLC (Agilent
644 Technologies) and the following gradient: 0–18 min, 5% B; 18–19 min, 95% B; 19–24 min, 95%
645 B; 24-25 min, 5% B; 25-40 min, 5% B where Buffer A was 0.1% formic acid and Buffer B was
646 0.1% formic acid in ACN. Flow rate was 0.18 mL min^{-1} and temperature was held constant at 25
647 °C. Compounds eluting from the column were analyzed with a 6560 Ion Mobility QTOF mass
648 spectrometer (Agilent Technologies) with the following settings: gas temp, 325 °C; drying gas,
649 12 L min^{-1}; nebulizer 55 psig; sheath gas temp 350 °C; sheath gas flow 10 L min^{-1}; capillary
650 voltage 4000 V; nozzle voltage 500 V; fragmentor 400 V. Retention times of (*S*)- and (*R*)-
651 norcoclaurine were established by comparison to an (*S*)-norcoclaurine authentic standard
652 (Toronto Research Chemicals Inc.) and *rac*-norcoclaurine, which was spontaneously condensed
653 from dopamine (Sigma) and 4-HPAA (Toronto Research Chemicals) in a KH_2PO_4/ACN buffer
654 (Pesnot et al., 2012). Retention times of (*S*)- and (*R*)-armepavine were established by comparison
655 to authentic (*R,S*)-armepavine standard and (*S*)-armepavine synthesized by a BY4741 yeast strain
656 harboring *Ps*6OMT, *Ps*CNMT, and *Nn*OMT5 (strain LP626) fed with (*S*)-norcoclaurine.

657 **Statistical analyses.** All numerical values are depicted as means ± s.d. Statistical differences
658 between control and engineered strains were assessed via two-tailed Student's *t*-tests assuming
659 equal variances using Excel (Microsoft) or Prism (GraphPad Software Inc.). In all cases, *P*-
660 values < 0.05 were considered significant.

661 # FIGURE LEGENDS

662 **Figure 1. *Nn*CYP80G is a stereospecific proaporphine synthase. a,** Proposed natural and
663 artificial routes to armepavine, glaziovine, and pronuciferine in sacred lotus and engineered
664 yeast, respectively. Lotus possesses five NCS isoforms for synthesis of (*R*)-norcoclaurine, which
665 is subsequently methylated to (*R*)-armepavine. Yeast strains utilized in this study employ a
666 truncated NCS variant from *C. japonica* (*Cj*NCSΔN), which yields exclusively (*S*)-
667 norcoclaurine. *Ps*6OMT, *Ps*CNMT, and *Nn*OMT5 (3× MTase) involved in the conversion of (*S*)-
668 norcoclaurine to (*S*)-armepavine are boxed. **b,** Analysis of BIA production by engineered strains.
669 Introduction of *Nn*OMT5 to strain LP603 enables high titer production of armepavine. Peak area
670 is shown for all pathway intermediates and absolute titers are depicted in mg/L for (*S*)-
671 norcoclaurine and (*S*)-armepavine. Asterisk (*) denotes a significant increase or decrease
672 ($P < 0.05$) in ion abundance relative to the parent strain. Error bars represent the mean ± s.d.
673 of $n = 3$ independent biological samples. Statistical differences between control and derivative
674 strains were tested using two-tailed Student's *t*-test. **c,** Chiral analysis of norcoclaurine and
675 armepavine synthesized *de novo* or from norcoclaurine-supplemented strains of yeast. Yeast-
676 derived norcoclaurine was compared against authentic (*S*)-norcoclaurine standard and (*R*,*S*)-
677 norcoclaurine generated by the phosphate-catalyzed condensation of dopamine and 4-HPAA.
678 Commercial (*S*)-norcoclaurine standard contains a small proportion of (*R*)-norcoclaurine, as
679 described previously (Pyne et al., 2020). Yeast-derived armepavine was compared against
680 authentic (*R*,*S*)-armepavine standard, sacred lotus extract, and (*S*)-armepavine generated from
681 feeding (*S*)-norcoclaurine to a BY4741 strain harboring *Ps*6OMT, *Ps*CNMT, and *Nn*OMT5 (3×
682 MTase). (*R*)-Conformers of norcoclaurine and armepavine are shaded. **d,** Ion-extracted LC–MS
683 chromatograms of engineered yeast strains harboring a partial pronuciferine pathway (*Ps*6OMT-

684 *Ps*CNMT-*Nn*OMT5-*Nn*CYP80G-*At*ATR2; LP626) fed with (*R*,*S*)-norcoclaurine, (*S*)-
685 norcoclaurine, or (*R*,*S*)-armepavine. LP626 is unable to synthesize BIAs *de novo* due to lack of
686 an NCS enzyme and a dopamine biosynthesis pathway. Retention time of yeast-derived
687 pronuciferine (dark blue) was compared against sacred lotus extract (light blue). **e,** MS/MS
688 fragmentation of pronuciferine from sacred lotus extract and strain LP626 fed with (*R,S*)-
689 norcoclaurine. Pronuciferine fragmentation is compared against two prior reports using authentic
690 pronuciferine standard (Bayazeid et al., 2018; Lin et al., 2014). **f,** Ion-extracted LC-MS
691 chromatograms of strain LP626 and its *NnOMT5*Δ derivative (LP627) fed with (*R*,*S*)-
692 norcoclaurine. Retention time of yeast-derived glaziovine (dark blue) was compared against
693 sacred lotus extract (light blue). **g,** MS/MS fragmentation of glaziovine from sacred lotus extract
694 and strain LP627 fed with (*R,S*)-norcoclaurine. Glaziovine fragmentation is compared against
695 two prior reports using authentic glaziovine standard (Cao et al., 2022; Yu et al., 2022).
696
697 **Figure 2. Screening poppy dehydroreticuline synthase (DRS) and dehydroreticuline**
698 **reductase (DRR) orthologs for *de novo* synthesis of pronuciferine from (*R*)-BIA**
699 **conformers. a,** Artificial *de novo* routes to (*R*)-*N*-methylcoclaurine and pronuciferine via
700 stereochemical inversion. (*S*)-Enantiomers are converted to corresponding 1,2-dehydro
701 intermediates using DRS, which are subsequently reduced to (*R*)-conformers using DRR. **b,**
702 Protein phylogenetic tree of DRS orthologs from various poppy species. Abbreviations: *Pr*,
703 *Papaver rhoeas* (common poppy); *Pb*, *Papaver bracteatum* (Iranian poppy); *Ps*, *Papaver*
704 *somniferum* (opium poppy); *Cm*, *Chelidonium majus* (greater celandine). **c,** Synthesis of 1,2-
705 dehydro-*N*-methylcoclaurine and 1,2-dehydroarmepavine by poppy DRS variants. DRS-
706 encoding genes were integrated into an (*S*)-armepavine-producing strain (LP609) and formation

707 of 1,2-dehydro intermediates was assayed by LC-MS. Asterisk (*) denotes a significant increase
708 or decrease ($P < 0.05$) in ion abundance relative to the precursor strain (LP609). **d,** Reduction of
709 1,2-dehydro-*N*-methylcoclaurine and 1,2-dehydroarmepavine by poppy DRR orthologs. Plasmid-
710 encoded DRR genes were introduced to LP609 harboring *Pr*DRS, *Nn*CYP80G, and *At*ATR2,
711 and consumption of 1,2-dehydro intermediates was assayed by LC-MS. *N*-Methylcoclaurine and
712 armepavine are reported as combined (*R*)- and (*S*)-conformers. Error bars represent the
713 mean ± s.d. of $n = 3$ independent biological samples. Asterisk (*) denotes a significant increase or
714 decrease ($P < 0.05$) in ion abundance relative to the precursor strain harboring *Pr*DRS,
715 *Nn*CYP80G, and *At*ATR2. Statistical differences between control and derivative strains were
716 tested using two-tailed Student's *t*-test. **e,** Chiral analysis of armepavine synthesized by strains
717 harboring *Pr*DRS or *Pr*DRS+*Ps*DRR. Implementation of *Pr*DRS+*Ps*DRR in conjunction with
718 *Nn*CYP80G+*At*ATR2 enables stereochemical inversion and concurrent synthesis of
719 pronuciferine. Pronuciferine was separated on a standard (non-chiral) C18 column.
720
721 **Figure 3. Combinatorial CYP80-CPR-CYB5 library for improved pronuciferine synthesis**
722 **and characterization of *Nn*CYP80A a,** Design of a partial 24-member CYP80-CPR-CYB5
723 combinatorial strain library. Two CYP80G variants (*Nn*CYP80G and *Ls*CYP80G) and CYP80A
724 from *N. nucifera* (*Nn*CYP80A) were paired with different combinations of plant cytochrome
725 P450 reductases (CPRs) and cytochrome *b5* (CYB5s) orthologs. The 24-strain library was
726 assayed with and without pHUM-PrDRS-PsDRR, which expresses *PrDRS* and *PsDRR* genes for
727 stereochemical inversion of BIA metabolites. Abbreviations: At, *Arabidopsis thaliana*; Cc2,
728 *Corydalis cheilanthifolia* CPR2; Cr, *Catharanthus roseus*; Ec, *Eschscholzia californica*; Hc,
729 *Hypericum calycinum*; *Pb*, *Papaver bracteatum*; *Ps*, *P. somniferum*. **b,** Pronuciferine production

730 by strains harboring *Nn*CYP80G or *Ls*CYP80G, pHUM-PrDRS-PsDRR, and different
731 combinations of CPR and CYB5. Asterisk (*) denotes a significant increase or decrease
732 ($P < 0.05$) in pronuciferine ion abundance between the designated strains. All strains exhibited a
733 significant increase ($P < 0.05$) in pronuciferine ion abundance relative to the parent strain lacking
734 a CYP80G, CPR, and CYB5. **c,** bis-BIA synthesis by strains harboring *Nn*CYP80A, pHUM-
735 PrDRS-PsDRR, and different combinations of CPR and CYB5. Asterisk (*) denotes a significant
736 increase or decrease ($P < 0.05$) in bis-BIA ion abundance between the designated strains. All
737 strains exhibited a significant increase ($P < 0.05$) in bis-BIA ion abundance relative to the parent
738 strain lacking *Nn*CYP80A, CPR, and CYB5. **d,** Proposed pathways to lotus bis-BIA alkaloids in
739 engineered yeast. *Nn*CYP80A catalyzes the stereospecific formation of nelumborine (C8-C3′) or
740 nelumboferine (C7-*O*-C3′) from *N*-methylcoclaurine via distinct phenol coupling routes.
741 Guattegaumerine biosynthesis in *Berberis stolonifera* is shown (boxed), which involves C3′-*O*-
742 C4′ coupling of two units of (*R*)-*N*-methylcoclaurine by *Bs*CYP80A1. **e,** Ion-extracted LC–MS
743 chromatograms of engineered yeast strains harboring *Nn*CYP80A or *Bs*CYP80A1, pHUM-
744 PrDRS-PsDRR, and a CPR. The bis-BIA product from *Nn*CYP80A-producing strains was
745 compared against commercial lotus extract. **f,** MS/MS fragmentation of a bis-BIA product (RT
746 ~5.2 min) from sacred lotus extract and strain LP625 containing *Nn*CYP80A and *At*ATR2. **g,**
747 MS/MS fragmentation of bis-BIA products (RT ~5.3 min) from strain LP625
748 (*Nn*CYP80A+*At*ATR2) and LP637 (*Bs*CYP80A1+*Hc*CPR). The 597 → 192 transition is the
749 major product observed upon fragmentation of authentic guattegaumerine standard (Payne et al.,
750 2021).
751

752 **Figure 4. Screening diverse plant *O*-methyltransferases for activity on nelumboferine. a,**
753 Proposed neferine biosynthesis pathways in *N. nucifera*. Neferine is synthesized via convergent
754 routes from liensinine or isoliensinine, both of which are presumed to arise from nelumboferine.
755 **b,** Protein phylogenetic tree of 66 *O*-methyltransferase orthologs from various plant species.
756 Abbreviations: *Am*, *Argemone mexicana*; *Cc*, *Corydalis cheilanthifolia*; *Cj*, *Coptis japonica*; *Cm*,
757 *Chelidonium majus*; *Cs*, *Corydalis saxicola*; *Ec*, *Eschscholzia californica*; *Gf*, *Glaucium flavum*;
758 *Hc*, *Hypericum calycinum*; *Nd*, *Nandina domestica*; *Nn*, *Nelumbo nucifera*; *Ns*, *Nigella sativa*;
759 *Pb*, *Papaver bracteatum*; *Ps*, *Papaver somniferum*; *Sc*, *Sanguinaria canadensis*; *Sd*, *Stylophorum*
760 *diphyllum*; *Tc*, *Tinospora cordifolia*; *Tf*, *Thalictrum flavum*; *Vh*, *Vancouveria hexandra*; Xs,
761 *Xanthoriza simplicissima.* **c,** Ion-extracted LC–MS chromatograms of engineered yeast strains
762 harboring *Nn*CYP80A, *At*ATR2, *Pr*DRS-*Ps*DRR, and *Ec*OMT1 from *Eschscholzia californica*.
763 Retention time of yeast-derived liensinine (dark blue) was compared against authentic liensinine
764 standard (black) and sacred lotus extract (green). **d,** MS/MS fragmentation of authentic liensinine
765 standard and a yeast strain engineered for liensinine synthesis (*Nn*CYP80A, ATR2, *Pr*DRS,
766 *Ps*DRR, and *Ec*OMT1). **e,** MS/MS fragmentation of tentative liensinine (RT = 2.16 min; dark
767 green) and isoliensinine (RT = 2.25 min; light green) products from commercial lotus extract.
768 Liensinine (611 → 206) and isoliensinine (611 → 192) yield different major fragment ions based
769 on a prior study (Zhou et al., 2007).

REFERENCES

Agnès, S. A., Okpekon, T., Kouadio, Y. A., Jagora, A., Bréard, D., Costa, E. V., da Silva, F., Koolen, H. H., Ray-Richomme, L., Richomme, P., 2022. Implementation of a MS/MS database for isoquinoline alkaloids and other annonaceous metabolites. Scientific Data. 9**,** 1-8.

Bai Flagfeldt, D., Siewers, V., Huang, L., Nielsen, J., 2009. Characterization of chromosomal integration sites for heterologous gene expression in *Saccharomyces cerevisiae*. Yeast. 26**,** 545-551.

Barton, D., Bhakuni, D., Chapman, G., Kirby, G., 1967. Phenol oxidation and biosynthesis. Part XV. The biosynthesis of roemerine, anonaine, and mecambrine. Journal of the Chemical Society C: Organic. 2134-2140.

Barton, D., Cohen, T., Some biogenetic aspects of phenol oxidation "Festschrift Prof. Dr. Arthur Stoll". Birkhäuser, Basel, 1957.

Bayazeid, O., Eylem, C. C., Reçber, T., Yalçın, F. N., Kır, S., Nemutlu, E., 2018. An LC-ESI-MS/MS method for the simultaneous determination of pronuciferine and roemerine in some *Papaver* species. J. Chromatogr. B. 1096**,** 223-227.

Bean, B. D., Whiteway, M., Martin, V. J. J., 2022. The MyLO CRISPR-Cas9 toolkit: a markerless yeast localization and overexpression CRISPR-Cas9 toolkit. G3. 12**,** jkac154.

Bishayee, A., Patel, P. A., Sharma, P., Thoutireddy, S., Das, N., 2022. Lotus (*Nelumbo nucifera* Gaertn.) and its bioactive phytocompounds: A tribute to cancer prevention and intervention. Cancers. 14**,** 529.

Bourgeois, L., Pyne, M. E., Martin, V. J., 2018. A highly characterized synthetic landing pad system for precise multicopy gene integration in yeast. ACS Synthetic Biology. 7**,** 2675-2685.

Cao, X., Lin, X., Wu, C., Zhang, M., Wang, M., 2022. Green extraction-assisted pseudo-targeted profile of alkaloids in Lotus seed epicarp based on UPLC-QTOF MS with IDA. Foods. 11**,** 1056.

Do, T. C. M. V., Nguyen, T. D., Tran, H., Stuppner, H., Ganzera, M., 2013. Analysis of alkaloids in Lotus (*Nelumbo nucifera* Gaertn.) leaves by non-aqueous capillary electrophoresis using ultraviolet and mass spectrometric detection. Journal of Chromatography A. 1302**,** 174-180.

Farrow, S. C., Hagel, J. M., Beaudoin, G. A., Burns, D. C., Facchini, P. J., 2015. Stereochemical inversion of (S)-reticuline by a cytochrome P450 fusion in opium poppy. Nature Chemical Biology. 11**,** 728-732.

Fossati, E., Narcross, L., Ekins, A., Falgueyret, J.-P., Martin, V. J. J., 2015. Synthesis of morphinan alkaloids in *Saccharomyces cerevisiae*. PloS One. 10**,** e0124459.

Fujii, N., Inui, T., Iwasa, K., Morishige, T., Sato, F., 2007. Knockdown of berberine bridge enzyme by RNAi accumulates (S)-reticuline and activates a silent pathway in cultured California poppy cells. Transgenic Research. 16**,** 363-375.

Galanie, S., Thodey, K., Trenchard, I. J., Interrante, M. F., Smolke, C. D., 2015. Complete biosynthesis of opioids in yeast. Science. 349**,** 1095-1100.

Grewal, P. S., Samson, J. A., Baker, J. J., Choi, B., Dueber, J. E., 2021. Peroxisome compartmentalization of a toxic enzyme improves alkaloid production. Nature Chemical Biology. 17**,** 96-103.

Haynes, L., Stuart, K., Barton, D., Bhakuni, D., Kirby, G., 1965. On the biosynthesis of crotonosine. Chemical Communications (London). 141-142.

He, C.-L., Huang, L.-Y., Wang, K., Gu, C.-J., Hu, J., Zhang, G.-J., Xu, W., Xie, Y.-H., Tang, N., Huang, A.-L., 2021. Identification of *bis*-benzylisoquinoline alkaloids as SARS-CoV-2 entry inhibitors from a library of natural products. Signal Transduction and Targeted Therapy. 6**,** 1-3.

Hong, B., Grzech, D., Caputi, L., Sonawane, P., López, C. E. R., Kamileen, M. O., Hernández Lozada, N. J., Grabe, V., O'Connor, S. E., 2022. Biosynthesis of strychnine. Nature. 607**,** 617-622.

Horwitz, A. A., Walter, J. M., Schubert, M. G., Kung, S. H., Hawkins, K., Platt, D. M., Hernday, A. D., Mahatdejkul-Meadows, T., Szeto, W., Chandran, S. S., 2015. Efficient multiplexed integration of synergistic alleles and metabolic pathways in yeasts via CRISPR-Cas. Cell Systems. 88-96.

Itoh, A., Saitoh, T., Tani, K., Uchigaki, M., Sugimoto, Y., Yamada, J., Nakajima, H., Ohshiro, H., Sun, S., Tanahashi, T., 2011. Bisbenzylisoquinoline alkaloids from *Nelumbo nucifera*. Chem. Pharm. Bull. 59**,** 947-951.

Jumper, J., Evans, R., Pritzel, A., Green, T., Figurnov, M., Ronneberger, O., Tunyasuvunakool, K., Bates, R., Žídek, A., Potapenko, A., 2021. Highly accurate protein structure prediction with AlphaFold. Nature. 596**,** 583-589.

Ka, S.-M., Kuo, Y.-C., Ho, P.-J., Tsai, P.-Y., Hsu, Y.-J., Tsai, W.-J., Lin, Y.-L., Shen, C.-C., Chen, A., 2010. (S)-armepavine from Chinese medicine improves experimental autoimmune crescentic glomerulonephritis. Rheumatology. 49**,** 1840-1851.

Kashiwada, Y., Aoshima, A., Ikeshiro, Y., Chen, Y.-P., Furukawa, H., Itoigawa, M., Fujioka, T., Mihashi, K., Cosentino, L. M., Morris-Natschke, S. L., 2005. Anti-HIV benzylisoquinoline alkaloids and flavonoids from the leaves of *Nelumbo nucifera*, and structure–activity correlations with related alkaloids. Bioorganic & Medicinal Chemistry. 13**,** 443-448.

Labuhn, M., Adams, F. F., Ng, M., Knoess, S., Schambach, A., Charpentier, E. M., Schwarzer, A., Mateo, J. L., Klusmann, J.-H., Heckl, D., 2017. Refined sgRNA efficacy prediction improves large-and small-scale CRISPR–Cas9 applications. Nucleic Acids Research. 46**,** 1375-1385.

Li, H., Yang, X., Zhang, Y., Gao, Z., Liang, Y., Chen, J., Shi, T., 2021. Nelumbo genome database, an integrative resource for gene expression and variants of *Nelumbo nucifera*. Scientific Data. 8**,** 1-7.

Lin, Z., Yang, R., Guan, Z., Chen, A., Li, W., 2014. Ultra-performance LC separation and quadrupole time-of-flight MS identification of major alkaloids in *Plumula Nelumbinis*. Phytochem. Anal. 25**,** 485-494.

Menéndez-Perdomo, I., Facchini, P., 2018. Benzylisoquinoline alkaloids biosynthesis in sacred lotus. Molecules. 23**,** 2899.

Menéndez-Perdomo, I. M., Facchini, P. J., 2020. Isolation and characterization of two *O*-methyltransferases involved in benzylisoquinoline alkaloid biosynthesis in sacred lotus (*Nelumbo nucifera*). J. Biol. Chem. 295**,** 1598-1612.

Mikkelsen, M. D., Buron, L. D., Salomonsen, B., Olsen, C. E., Hansen, B. G., Mortensen, U. H., Halkier, B. A., 2012. Microbial production of indolylglucosinolate through engineering of a multi-gene pathway in a versatile yeast expression platform. Metabolic Engineering. 14**,** 104-111.

Morris, J. S., Facchini, P. J., 2019. Molecular origins of functional diversity in benzylisoquinoline alkaloid methyltransferases. Frontiers in Plant Science. 10**,** 1058.
Nelson, D. R., Schuler, M. A., 2013. Cytochrome P450 genes from the sacred lotus genome. Tropical plant biology. 6**,** 138-151.
Nett, R. S., Lau, W., Sattely, E. S., 2020. Discovery and engineering of colchicine alkaloid biosynthesis. Nature. 584**,** 148-153.
Nishibe, S., Tsukamoto, H., Kinoshita, H., Kitagawa, S., Sakushima, A., 1986. Alkaloids from embryo of the seed of *Nelumbo nucifera*. Journal of Natural Products. 49**,** 547-548.
Nishimura, K., Horii, S., Tanahashi, T., Sugimoto, Y., Yamada, J., 2013. Synthesis and pharmacological activity of alkaloids from embryo of lotus, *Nelumbo nucifera*. Chemical and Pharmaceutical Bulletin. 61**,** 59-68.
Payne, J. T., Valentic, T. R., Smolke, C. D., 2021. Complete biosynthesis of the bisbenzylisoquinoline alkaloids guattegaumerine and berbamunine in yeast. Proceedings of the National Academy of Sciences. 118**,** e2112520118.
Pesnot, T., Gershater, M. C., Ward, J. M., Hailes, H. C., 2012. The catalytic potential of *Coptis japonica* NCS2 revealed–Development and utilisation of a fluorescamine-based assay. Advanced Synthesis & Catalysis. 354**,** 2997-3008.
Purwanto, R., Hori, K., Yamada, Y., Sato, F., 2017. Unraveling additional O-methylation steps in benzylisoquinoline alkaloid biosynthesis in California poppy (*Eschscholzia californica*). Plant and Cell Physiology. 58**,** 1528-1540.
Pyne, M., Narcross, L., Fossati, E., Bourgeois, L., Burton, E., Gold, N., Martin, V., 2016. Reconstituting plant secondary metabolism in *Saccharomyces cerevisiae* for production of high-value benzylisoquinoline alkaloids. Methods in enzymology.
Pyne, M. E., Kevvai, K., Grewal, P. S., Narcross, L., Choi, B., Bourgeois, L., Dueber, J. E., Martin, V. J. J., 2020. A yeast platform for high-level synthesis of tetrahydroisoquinoline alkaloids. Nat. Commun. 11**,** 1-10.
Pyne, M. E., Martin, V. J., 2022. Microbial synthesis of natural, semisynthetic, and new-to-nature tetrahydroisoquinoline alkaloids. Current Opinion in Green and Sustainable Chemistry. 33**,** 100561.
Reider Apel, A., d'Espaux, L., Wehrs, M., Sachs, D., Li, R. A., Tong, G. J., Garber, M., Nnadi, O., Zhuang, W., Hillson, N. J., 2016. A Cas9-based toolkit to program gene expression in *Saccharomyces cerevisiae*. Nucleic Acids Research. 45**,** 496-508.
Ryan, O. W., Skerker, J. M., Maurer, M. J., Li, X., Tsai, J. C., Poddar, S., Lee, M. E., DeLoache, W., Dueber, J. E., Arkin, A. P., 2014. Selection of chromosomal DNA libraries using a multiplex CRISPR system. Elife. 3**,** e03703.
Shao, Z., Zhao, H., Zhao, H., 2009. DNA assembler, an *in vivo* genetic method for rapid construction of biochemical pathways. Nucleic Acids Research. 37**,** e16-e16.
Smith, J. D., Suresh, S., Schlecht, U., Wu, M., Wagih, O., Peltz, G., Davis, R. W., Steinmetz, L. M., Parts, L., Onge, R. P. S., 2016. Quantitative CRISPR interference screens in yeast identify chemical-genetic interactions and new rules for guide RNA design. Genome biology. 17**,** 45.
Stuart, K., Cava, M., 1968. Proaporphine alkaloids. Chemical Reviews. 68**,** 321-339.
Varadi, M., Anyango, S., Deshpande, M., Nair, S., Natassia, C., Yordanova, G., Yuan, D., Stroe, O., Wood, G., Laydon, A., 2022. AlphaFold Protein Structure Database: massively expanding the structural coverage of protein-sequence space with high-accuracy models. Nucleic acids research. 50**,** D439-D444.

Winzer, T., Kern, M., King, A. J., Larson, T. R., Teodor, R. I., Donninger, S. L., Li, Y., Dowle, A. A., Cartwright, J., Bates, R., 2015. Morphinan biosynthesis in opium poppy requires a P450-oxidoreductase fusion protein. Science. 349**,** 309-312.

Yang, G.-M., Sun, J., Pan, Y., Zhang, J.-L., Xiao, M., Zhu, M.-S., 2018. Isolation and identification of a tribenzylisoquinoline alkaloid from *Nelumbo nucifera* Gaertn, a novel potential smooth muscle relaxant. Fitoterapia. 124**,** 58-65.

Yang, M., Zhu, L., Li, L., Li, J., Xu, L., Feng, J., Liu, Y., 2017. Digital gene expression analysis provides insight into the transcript profile of the genes involved in aporphine alkaloid biosynthesis in lotus (*Nelumbo nucifera*). Frontiers in Plant Science. 8**,** 80.

Yu, Y., Wei, X., Liu, Y., Dong, G., Hao, C., Zhang, J., Jiang, J., Cheng, J., Liu, A., Chen, S., 2022. Identification and quantification of oligomeric proanthocyanidins, alkaloids, and flavonoids in lotus seeds: A potentially rich source of bioactive compounds. Food Chemistry. 379**,** 132124.

Zhou, H., Jiang, H., Yao, T., Zeng, S., 2007. Fragmentation study on the phenolic alkaloid neferine and its analogues with anti-HIV activities by electrospray ionization tandem mass spectrometry with hydrogen/deuterium exchange and its application for rapid identification of in vitro microsomal metabolites of neferine. Rapid Communications in Mass Spectrometry: An International Journal Devoted to the Rapid Dissemination of Up-to-the-Minute Research in Mass Spectrometry. 21**,** 2120-2128.

Zhou, J., Li, G., Zheng, Y., Shen, H.-M., Hu, X., Ming, Q.-L., Huang, C., Li, P., Gao, N., 2015. A novel autophagy/mitophagy inhibitor liensinine sensitizes breast cancer cells to chemotherapy through DNM1L-mediated mitochondrial fission. Autophagy. 11**,** 1259-1279.

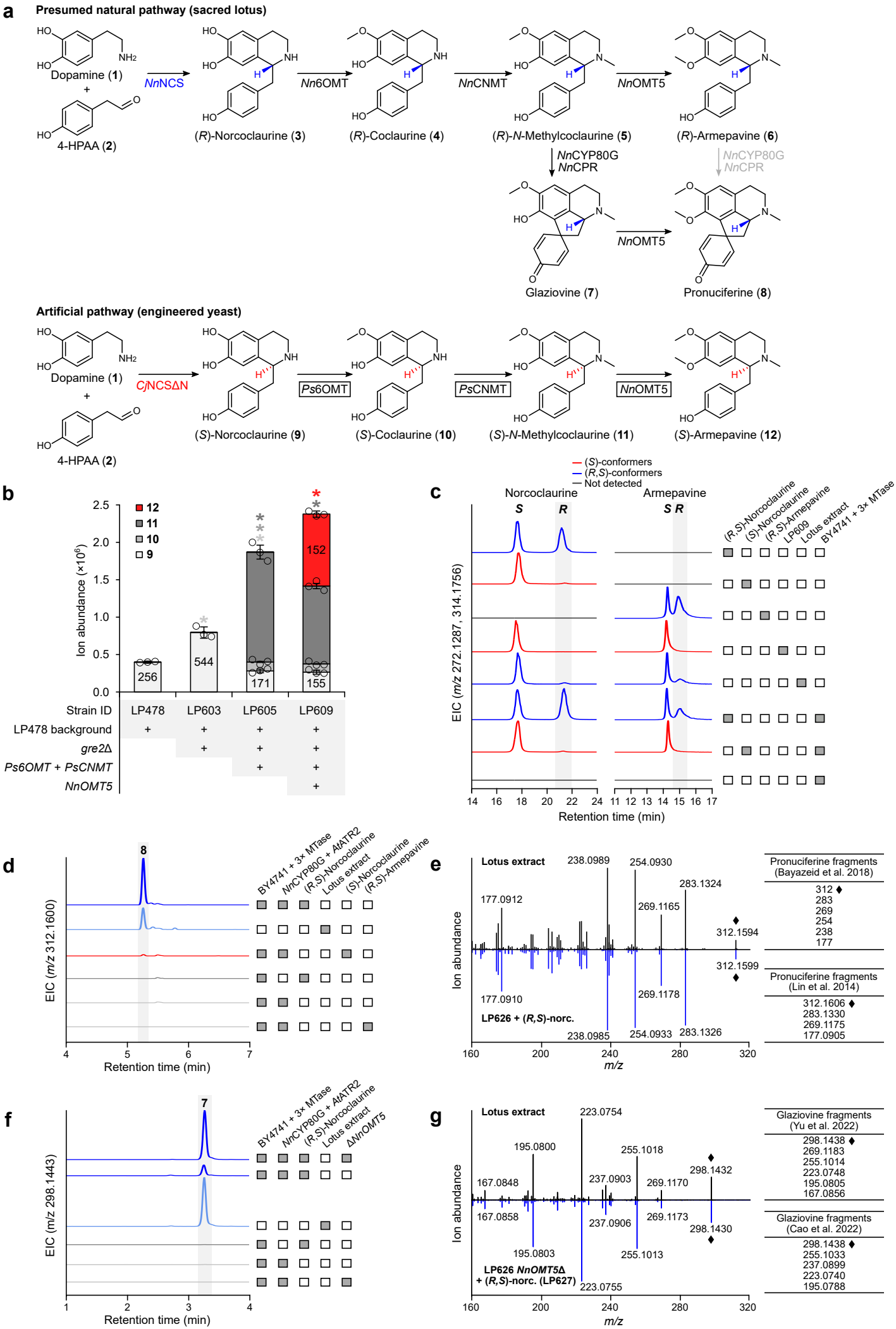
a
Presumed natural pathway (sacred lotus)
Dopamine (1)
4-HPAA (2)
NnNCS
(R)-Norcoclaurine (3)
Nn6OMT
(R)-Coclaurine (4)
NnCNMT
(R)-N-Methylcoclaurine (5)
NnOMT5
(R)-Armepavine (6)
NnCYP80G
NnCPR
Glaziovine (7)
Pronuciferine (8)
Artificial pathway (engineered yeast)
CjNCSΔN
(S)-Norcoclaurine (9)
Ps6OMT
(S)-Coclaurine (10)
PsCNMT
(S)-N-Methylcoclaurine (11)
(S)-Armepavine (12)
b
Ion abundance (×10^6)
12
11
10
9
256
544
171
155
152
Strain ID
LP478
LP603
LP605
LP609
LP478 background
gre2Δ
Ps6OMT + PsCNMT
NnOMT5
c
(S)-conformers
(R,S)-conformers
Not detected
Norcoclaurine
Armepavine
EIC (m/z 272.1287, 314.1756)
Retention time (min)
(R,S)-Norcoclaurine
(S)-Norcoclaurine
(R,S)-Armepavine
LP609
Lotus extract
BY4741 + 3× MTase
d
EIC (m/z 312.1600)
Retention time (min)
BY4741 + 3× MTase
NnCYP80G + AtATR2
(R,S)-Norcoclaurine
Lotus extract
(S)-Norcoclaurine
(R,S)-Armepavine
e
Lotus extract
LP626 + (R,S)-norc.
Ion abundance
m/z
Pronuciferine fragments (Bayazeid et al. 2018)
Pronuciferine fragments (Lin et al. 2014)
f
EIC (m/z 298.1443)
Retention time (min)
BY4741 + 3× MTase
NnCYP80G + AtATR2
(R,S)-Norcoclaurine
Lotus extract
ΔNnOMT5
g
Lotus extract
LP626 NnOMT5Δ + (R,S)-norc. (LP627)
Ion abundance
m/z
Glaziovine fragments (Yu et al. 2022)
Glaziovine fragments (Cao et al. 2022)

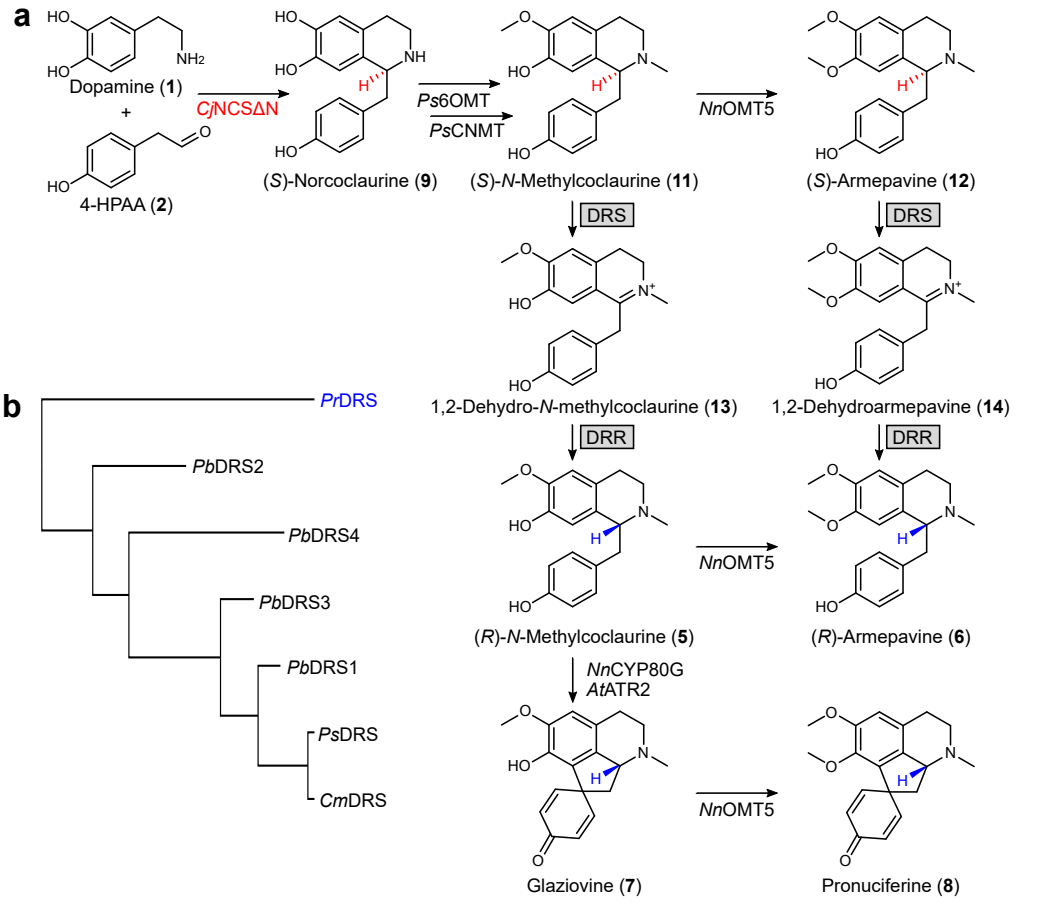
a
Dopamine (1)
4-HPAA (2)
CjNCSΔN
(S)-Norcoclaurine (9)
Ps6OMT
PsCNMT
(S)-N-Methylcoclaurine (11)
NnOMT5
(S)-Armepavine (12)
DRS
1,2-Dehydro-N-methylcoclaurine (13)
1,2-Dehydroarmepavine (14)
DRR
(R)-N-Methylcoclaurine (5)
(R)-Armepavine (6)
NnCYP80G
AtATR2
Glaziovine (7)
Pronuciferine (8)
b
PrDRS
PbDRS2
PbDRS4
PbDRS3
PbDRS1
PsDRS
CmDRS

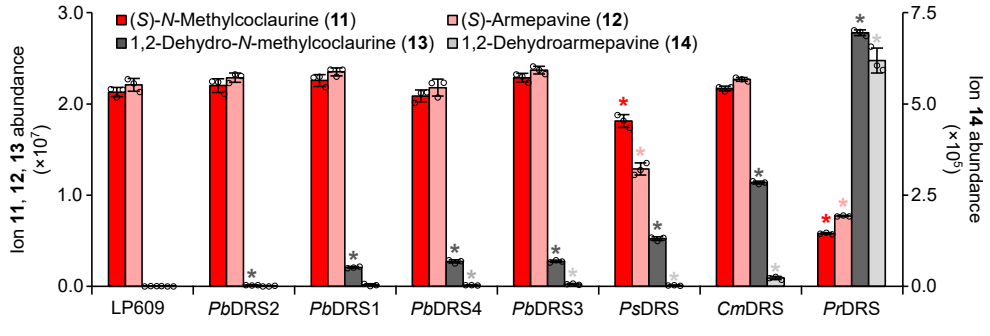
c
(S)-N-Methylcoclaurine (11)
(S)-Armepavine (12)
1,2-Dehydro-N-methylcoclaurine (13)
1,2-Dehydroarmepavine (14)
Ion 11, 12, 13 abundance (×10^7)
Ion 14 abundance (×10^5)
LP609
PbDRS2
PbDRS1
PbDRS4
PbDRS3
PsDRS
CmDRS
PrDRS

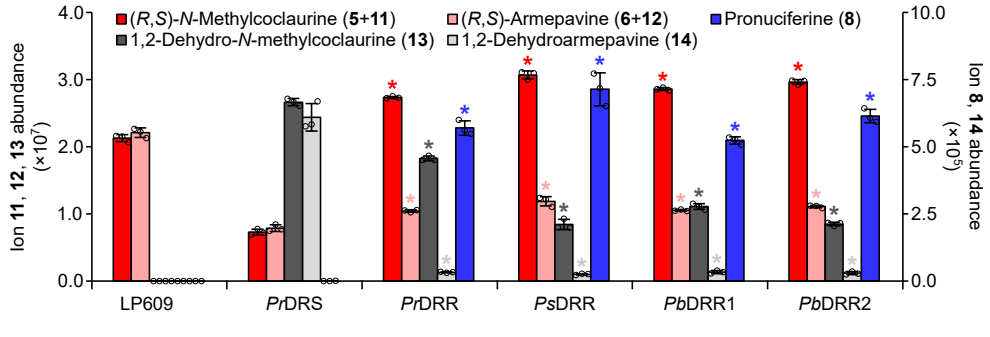
d
(R,S)-N-Methylcoclaurine (5+11)
(R,S)-Armepavine (6+12)
Pronuciferine (8)
1,2-Dehydro-N-methylcoclaurine (13)
1,2-Dehydroarmepavine (14)
Ion 11, 12, 13 abundance (×10^7)
Ion 8, 14 abundance (×10^5)
LP609
PrDRS
PrDRR
PsDRR
PbDRR1
PbDRR2

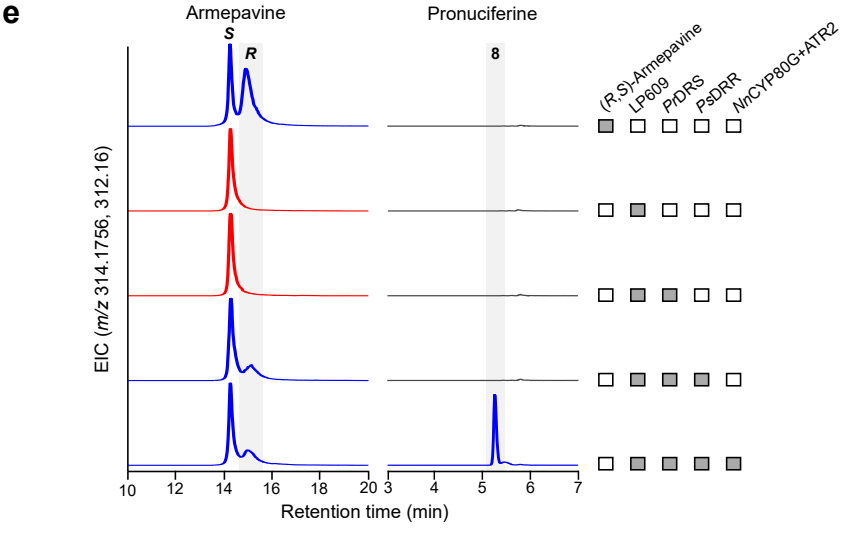
e
Armepavine
Pronuciferine
S
R
8
(R,S)-Armepavine
LP609
PrDRS
PsDRR
NnCYP80G+ATR2
EIC (m/z 314.1756, 312.16)
Retention time (min)

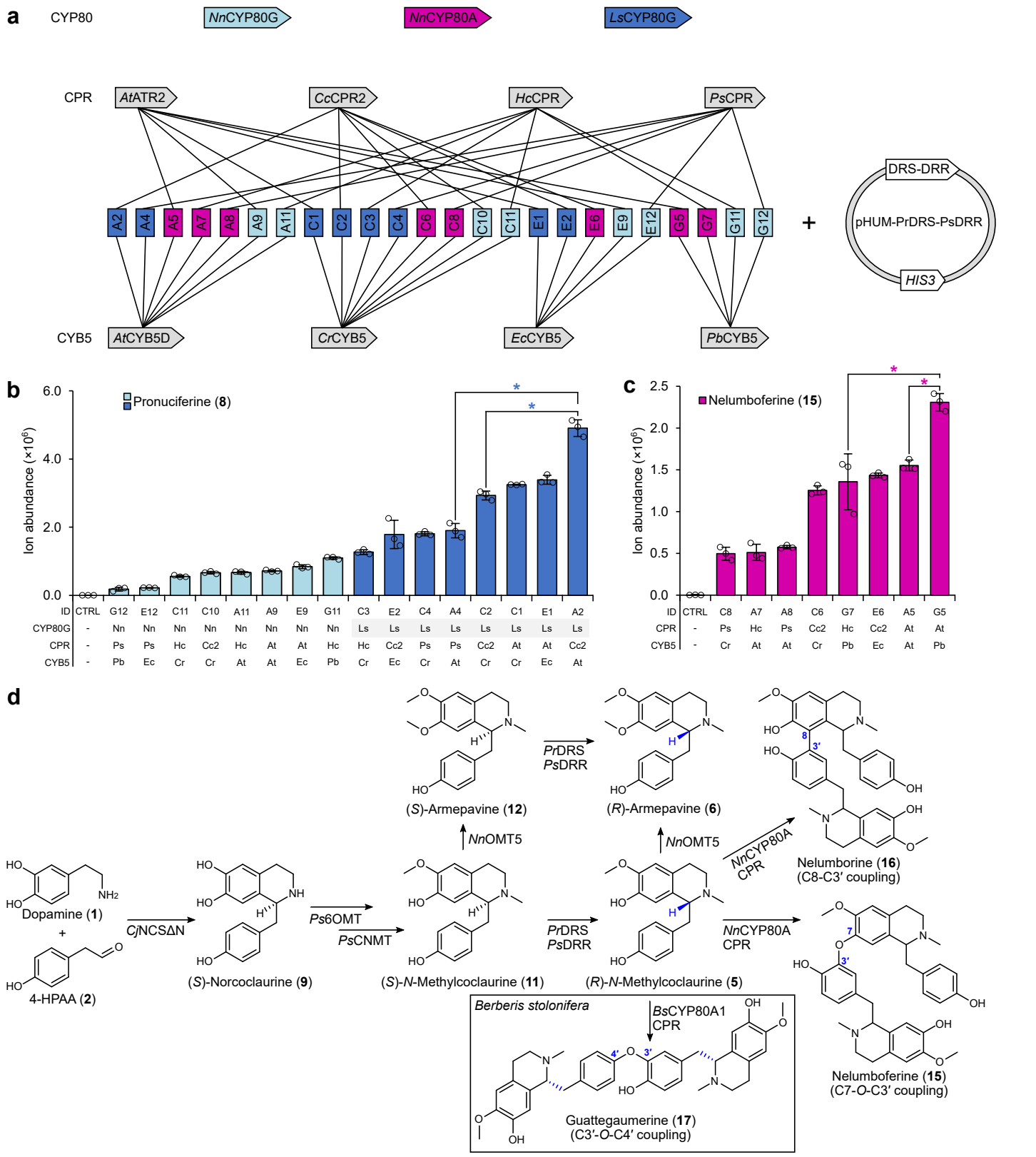
a
CYP80
NnCYP80G
NnCYP80A
LsCYP80G
CPR
AtATR2
CcCPR2
HcCPR
PsCPR
A2 A4 A5 A7 A8 A9 A11 C1 C2 C3 C4 C6 C8 C10 C11 E1 E2 E6 E9 E12 G5 G7 G11 G12
+
DRS-DRR
pHUM-PrDRS-PsDRR
HIS3
CYB5
AtCYB5D
CrCYB5
EcCYB5
PbCYB5
b
Pronuciferine (8)
Ion abundance (×10^6)
ID CTRL G12 E12 C11 C10 A11 A9 E9 G11 C3 E2 C4 A4 C2 C1 E1 A2
CYP80G - Nn Nn Nn Nn Nn Nn Nn Nn Ls Ls Ls Ls Ls Ls Ls Ls
CPR - Ps Ps Hc Cc2 Hc At At Hc Hc Cc2 Ps Ps Cc2 At At Cc2
CYB5 - Pb Ec Cr Cr At At Ec Pb Cr Ec Cr At Cr Cr Ec At
c
Nelumboferine (15)
Ion abundance (×10^6)
ID CTRL C8 A7 A8 C6 G7 E6 A5 G5
CPR - Ps Hc Ps Cc2 Hc Cc2 At At
CYB5 - Cr At At Cr Pb Ec At Pb
d
Dopamine (1)
4-HPAA (2)
CjNCSΔN
(S)-Norcoclaurine (9)
Ps6OMT
PsCNMT
(S)-N-Methylcoclaurine (11)
NnOMT5
(S)-Armepavine (12)
PrDRS
PsDRR
(R)-N-Methylcoclaurine (5)
(R)-Armepavine (6)
NnCYP80A
CPR
Nelumborine (16)
(C8-C3′ coupling)
Nelumboferine (15)
(C7-O-C3′ coupling)
Berberis stolonifera
BsCYP80A1
CPR
Guattegaumerine (17)
(C3′-O-C4′ coupling)
e
5.2 min
5.3 min
LP609
NnOMT5
NnCYP80A + ATR2
pHUM-PrDRS-PsDRR
Lotus extract
BsCYP80A + HcCPR
EIC (m/z 597.2965)
Retention time (min)
f
LP625 (NnCYP80A+ATR2)
RT 5.21 min, 25 V
Lotus extract
RT 5.22 min, 25 V
Ion abundance
m/z
g
LP625 (NnCYP80A+ATR2)
RT 5.31 min, 25 V
LP637 (BsCYP80A1+HcCPR)
RT 5.31 min, 25 V
Ion abundance
m/z

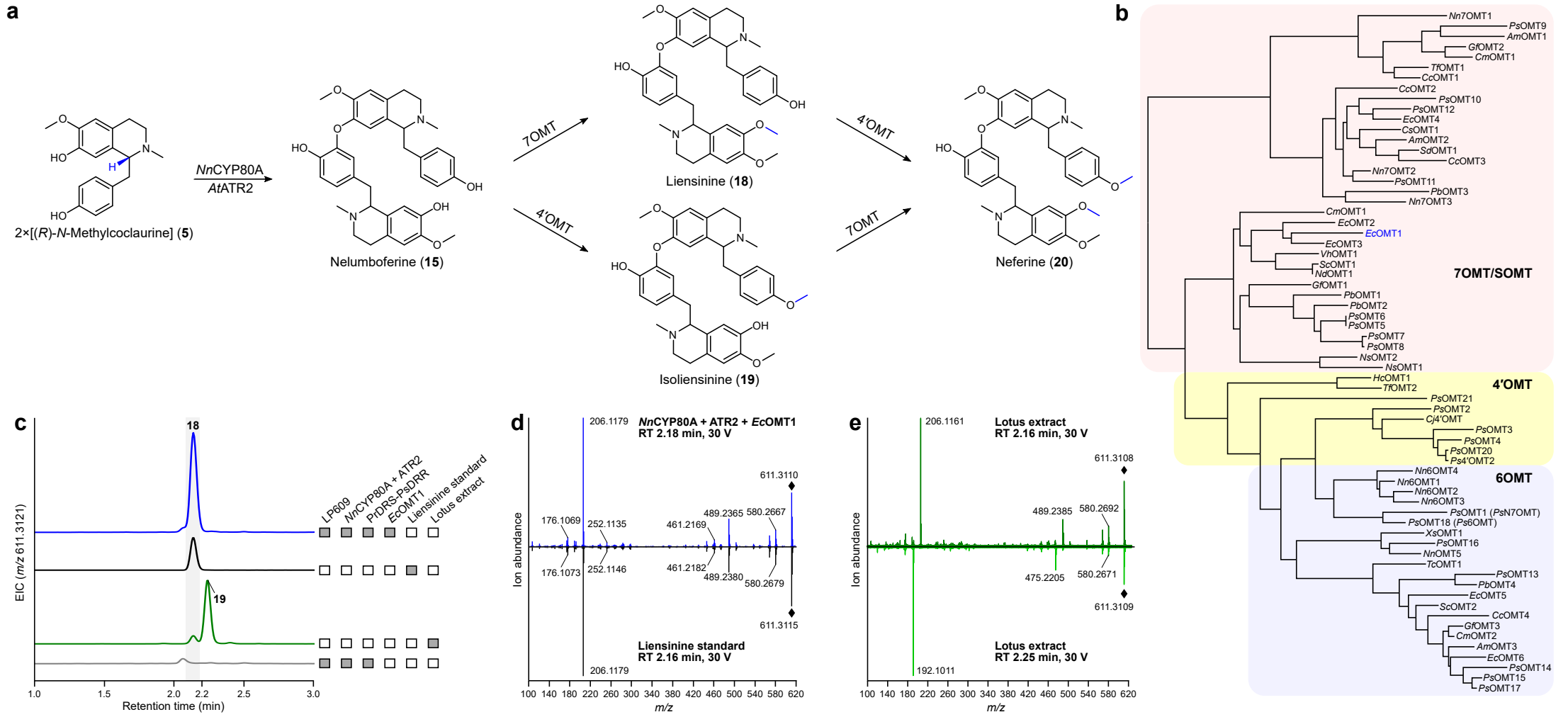
a
2×[(R)-N-Methylcoclaurine] (5)
NnCYP80A
AtATR2
Nelumboferine (15)
7OMT
4'OMT
Liensinine (18)
Isoliensinine (19)
4'OMT
7OMT
Neferine (20)
b
7OMT/SOMT
4'OMT
6OMT
c
EIC (m/z 611.3121)
Retention time (min)
LP609
NnCYP80A + ATR2
PrDRS-PsDRR
EcOMT1
Liensinine standard
Lotus extract
d
NnCYP80A + ATR2 + EcOMT1
RT 2.18 min, 30 V
Liensinine standard
RT 2.16 min, 30 V
Ion abundance
m/z
e
Lotus extract
RT 2.16 min, 30 V
Lotus extract
RT 2.25 min, 30 V
Ion abundance
m/z